Article

Not peer-reviewed version

Marf and Opa1-Dependent Formation of Mitochondrial Network Structure Is Required for Cell Growth and the Subsequent Meiosis in *Drosophila* Males

Tatsuru Matsuo , Mitsuki Yamanaka , Yoshihiro H. Inoue *

Posted Date: 3 September 2025

doi: 10.20944/preprints202509.0318.v1

Keywords: mitochondrial dynamics; drosophila; meiosis; spermatogenesis; Cyclin B; Nebenkern

 doi:10.20944/preprints202509.0318.v1

Article

Marf and Opa1-Dependent Formation of Mitochondrial Network Structure Is Required for Cell Growth and the Subsequent Meiosis in *Drosophila* Males

Tatsuru Matsuo, Mitsuki Yamanaka and Yoshihiro H. Inoue *

Biomedical Research Center, Kyoto Institute of Technology, Matsugasaki, Sakyo-ku, Kyoto, 606-0962, Japan

* Correspondence: yhinoue@kit.ac.jp; Tel.:+81-75-(724)7876

Abstract

Mitochondria are dynamic organelles that undergo repeated fusion and fission. We studied how the distribution and shape of mitochondria change during *Drosophila* spermatogenesis and whether factors that regulate their dynamics are necessary for these changes. Unlike the shortened mitochondria seen in mitosis, an interconnected network of elongated mitochondria forms before meiosis and is maintained during meiotic divisions. Mitochondria are evenly divided into daughter cells, relying on microtubules and F-actin. To explore the role of mitochondrial network structure in cell growth and meiosis, we depleted mitochondrial fusion factors, Opa1 and Marf, as well as the morphology proteins Letm1 and EndoB, in spermatocytes. This knockdown led to inhibited cell growth and failed meiosis. As a result, the spermatocytes differentiated into spermatids without completing meiosis. The knockdown also inhibited the cytoplasmic and nuclear accumulation of Cyclin B before meiosis, and Cdk1 was not fully activated at the onset of meiosis. Notably, ectopic overexpression of Cyclin B partially rescued the failure of meiosis. Many spermatids from spermatocytes with the knockdowns contained multiple smaller nuclei and abnormally shaped Nebenkerns. These findings suggest that mitochondrial network structure, maintained by fusion and morphology factors, is essential for meiosis progression and Nebenkern formation in *Drosophila* spermatogenesis.

Keywords: mitochondrial dynamics; drosophila; meiosis; spermatogenesis; Cyclin B; Nebenkern

1. Introduction

Mitochondria have been depicted as granular capsule-like structures based on past transmission electron microscope images, but in addition to the structures, they exhibit various morphological forms, including filamentous and rod-shaped structures, and interconnected structures made of elongated mitochondria called network structure (Bereiter-Hahn and Vöth, 1994; Labbé and Murley, 2014; Hinton et al., 2023). The diversity and changes in their architectures have been proposed based on observations made using light microscopy (Bereiter-Hahn and Vöth, 1994), and these findings have recently been confirmed by those with super-resolution microscopy and three-dimensional high-resolution electron microscopy (Hinton, et al., 2023; Stephan, et al., 2024). When oxidative damages are generated in mitochondria, fusion between neighboring mitochondria allows damaged proteins and DNA to be replaced with normal ones from other mitochondria, and metabolic products to be shared (Chen et al., 2010). Damaged mitochondria undergo fission, and the smaller sections with the damaged parts are broken down and eliminated by mitophagy. Fusion and fission are essential for maintaining the function of mitochondria within cells (Sauvanet et al., 2010; Benard et al., 2007). Even during normal cell proliferation, the morphology changes depending on the phase of the cell cycle (Madan et al., 2022). The elongated structures formed via the fusion of multiple

 doi:10.20944/preprints202509.0318.v1

mitochondria during interphase in mammalian cells transform into granular structures just before entering M-phase. At the end of M-phase, these elongated structures are reassembled. The ability of mitochondria to take on different shapes was postulated to be related to their dynamic nature involving repeated fusion and fission (Bereiter-Hahn and Vöth, 1994). However, no direct evidence has been provided to show that the factors controlling mitochondrial fusion and fission influence these shape changes.

The studies on the molecular mechanisms that regulate mitochondrial morphogenesis commenced with the isolation of mitochondrial morphogenesis-deficient mutants in budding yeast (Okamoto and Shaw, 2005). Three GTPases essential for mitochondrial fusion and fission were originally identified: the cytoplasmic dynamin-related GTPase, Drp1, plays a key role in mitochondrial fission, while Mfn1/2 functions in the outer membrane fusion of mitochondria, and Opa1 in the inner membrane fusion of mitochondria. Orthologs for those small GTPases have been identified in *Drosophila* and mammals (Hales and Fuller 1997; Eura et al., 2003; Deng et al., 2008). If these factors do not function properly, the balance between fusion and fission is disturbed, which can impact mitochondrial morphogenesis and function. In addition, LETM1 is a mitochondria inner membrane protein that is required for mitochondria morphology and cristae structures (Nakamura et al., 2020). Disrupting mammalian Endophilin B1, which is located on the outer membrane of mitochondria, also causes abnormal elongation of the outer mitochondrial membrane and disturbs the balance between fusion and fission (Karbowski et al., 2004). Here, we refer to these two membrane proteins as mitochondrial morphology proteins and studied them together with the fusion and fission factors. It is becoming increasingly clear that mitochondrial morphology is closely associated with important biological phenomena, including the cell cycle, apoptosis, starvation response, and developmental events (Zhao et al., 2013). Some proteins involved in mitochondrial morphology have been reported to play a crucial role in mouse embryogenesis and brain development: mice lacking the fusion and fission factors, *mfn1* (*mitofusin 1*), *mfn2* (*mitofusin 2*), *Opa1* (*optic atrophy 1*), and *Drp1* (*dynamin-related protein 1*), are lethal in the early stages of embryogenesis (Liesa et al., 2009, Chen et al., 2003, Davies et al., 2007, Ishihara et al., 2009, Wakabayashi et al., 2009). These reports suggest that mitochondrial dynamics play a crucial role in embryonic and neural development. However, it remains unclear whether mitochondrial morphological changes, especially the formation of mitochondrial networks, are necessary for the development of other tissues.

The morphology of mitochondria undergoes remarkable changes during spermatogenesis in *Drosophila* (Fuller, 1993; Ichihara et al., 2007; Inoue et al., 2012; Vedelek et al., 2024). The spermatogenesis process begins with the asymmetric division of germline stem cells localized at the testis tip. Of their two daughter cells, one becomes a spermatogonium destined for differentiation and undergoes four rounds of mitosis, resulting in the production of 16 primary spermatocytes. These cells form a cell unit designated as a cyst, and thereafter, these 16 cells synchronously undergo a remarkable growth during the cell growth phase, which is divided into seven phases: S1 (premeiotic DNA replication phase), S2a, S2b, S3 to S6 (Cenci et al., 1994; Inoue et al., 2012). The cells at each stage can be easily distinguished by their size and the intracellular distribution of Sa protein. (Inoue, et al., 2012; Azuma et al., 2021). The cells in the S2b stage are characterized by a polar distribution of the nucleus and mitochondrial aggregates adjacent to the nucleus. Thereafter, in the S3-5 stage, when the nucleus is localized at the center of the cells, mitochondria are dispersed through the cytoplasm. At the S6 stage, at the end of the growth phase, spermatocytes reach their maximum size. These characteristics make the cells at each stage easier to identify. After the spermatocyte completes the growth phase, it undergoes two consecutive meiotic divisions. In meiotic cells, mitochondria are diffused into the cytoplasm at the onset of prophase I and align along aster microtubules (Fuller, 1993; Inoue, 2012). Mitochondria are then clustered between two facing asters and are then distributed along the central spindle microtubules. Mitochondria detach from the microtubule structure and spread throughout the cytoplasm at the end of meiosis I. Second meiosis proceeds in the same manner, resulting in the production of 64 spermatids (Ichihara et al., 2007). Mitochondria in a post-meiotic cell, designated a spermatid, construct a large and spherical aggregate known as a

 doi:10.20944/preprints202509.0318.v1

Nebenkern next to the nucleus. Thus, as mitochondria form a noticeable structure in the post-meiotic cells, abnormalities that result from mitochondrial morphology and distribution in meiosis can be easily recognized.

In *Drosophila,* two orthologues of the mammalian mitochondrial outer membrane fusion factors are expressed. One is *Marf*, which is ubiquitously expressed through development in *Drosophila*, and the other is *fzo* (*fuzzy onion*), which is expressed specifically in male germ cells. The *fzo* mutants form multiple small Nebenkerns (Hales and Fuller, 1997). Similar abnormalities in Nebenkern formation have been reported in mutant spermatocytes for *Opa1,* responsible for inner membrane fusion (McQuibban et al., 2006). The cells lacking *Drp1,* encoding a mitochondrial fission factor, also display a similar Nebenkern phenotype (Aldridge et al., 2007). These findings suggest that both mitochondrial fusion and fission factors are required for the Nebenkern formation. Abnormal Nebenkerns may arise from abnormalities in the process where mitochondria fuse to create two giant organelles. Alternatively, it may be issues in the distribution or structure of mitochondria before or during meiotic divisions. The fine morphology and distribution of mitochondria before and during meiosis, as well as the regulatory factors involved in these processes, remain to be investigated.

In this study, we focused on morphological changes of mitochondria during *Drosophila* spermatogenesis, especially before and during meiosis. We investigated whether the mitochondrial fusion factors, Marf and Opa1, are required for the formation of a network structure consisting of the elongated mitochondria. In addition, we investigated whether the morphology proteins, Letm1 and EndoB, are also required for the mitochondrial morphological changes. Moreover, we investigated whether the mitochondrial network structure constructed via these gene products plays an indispensable role in male meiosis. We also address the mechanism underlying the fact that the knockdown of the fusion genes essential for the network structure inhibits meiosis. Since mitochondria are essential organelles in spermatogenesis, not only in *Drosophila* but also in mammals, our findings may provide important insights into the roles of mitochondrial dynamics in spermatogenesis.

2. Results

2.1. Differences in Mitochondrial Morphology and Distribution in Spermatogonia That Proliferate via Mitosis, Spermatocytes Before and During Male Meiosis in Drosophila

To compare fine structures of mitochondria during germ line cell development in the *Drosophila* males, the testis cells were immunostained with an antibody against mitochondrial ATP synthetase and observed by confocal microscopy. During mitosis of a spermatogonium arising from a germline stem cell, mitochondria were distributed in the cytoplasm of daughter cells in a dot-like morphology (arrowheads in Figure 1A′, B′). During the interphase when an aster was localized on the nuclear membrane, mitochondria diffused into the cytoplasm in granular and interconnected forms (arrow in Figure 1C′). 16 spermatogonia generated via four rounds of mitosis form a single cell unit, a cyst, and undergo cell growth synchronously. During an early stage (S2b) of the cell growth phase, elongated mitochondria were accumulated next to the nucleus (arrows in Figure 1D, see the super-resolution microscopic images in Figure S1A′, A″). As the development of spermatocytes progressed from the S2b to the S3-S5 stages, the mitochondrial network transformed to a granular and shortened form (Figure 1E, see Figure S1B′, B″). By the mature stage (S6), just before the onset of meiosis, the network structure consisted of elongated mitochondria was constructed (arrows in Figure S1D′, D″, arrow in the inset of Figure 1F′). During meiosis I, this network structure was maintained and distributed around aster microtubules (Figure 1G). By metaphase I, mitochondria had migrated toward the plus ends and were assembled along the vicinity of the plasma membrane to the cell equator between the two asters (Figure 1H, see t=10-40 min in live analysis in Figure S2). At this stage, the mitochondrial network structure was not fragmented or distributed, while retaining its original structure (see Figure S1E, F). In late anaphase I, as central spindle microtubules were formed between daughter nuclei, mitochondria shifted from near the plasma membrane to the center, where these

 doi:10.20944/preprints202509.0318.v1

microtubules are located (arrows in Figure 1I'). By the end of anaphase I, mitochondria are distributed in a ribbon-like shape on the central spindle (Figure 1J'). As the spindle structure disintegrated during telophase I, mitochondria continued to be distributed in the shape (Figure 1K). Furthermore, we confirmed the presence of the elongated mitochondria in anaphase I to telophase I by transmission electron microscopy (Figure S1G, G', H, and H'). After the cytokinesis of the first meiotic division was completed, mitochondria appeared to diffuse into the cytoplasm as the microtubule structure disintegrated. At this stage, mitochondria were dispersed into the cytoplasm while keeping an elongated network structure (inset in Figure 1L'). Mitochondria were distributed in the same manner in the second meiosis. After the completion of meiosis, mitochondria formed a single aggregate, known as a Nebenkern (Figure 1M).

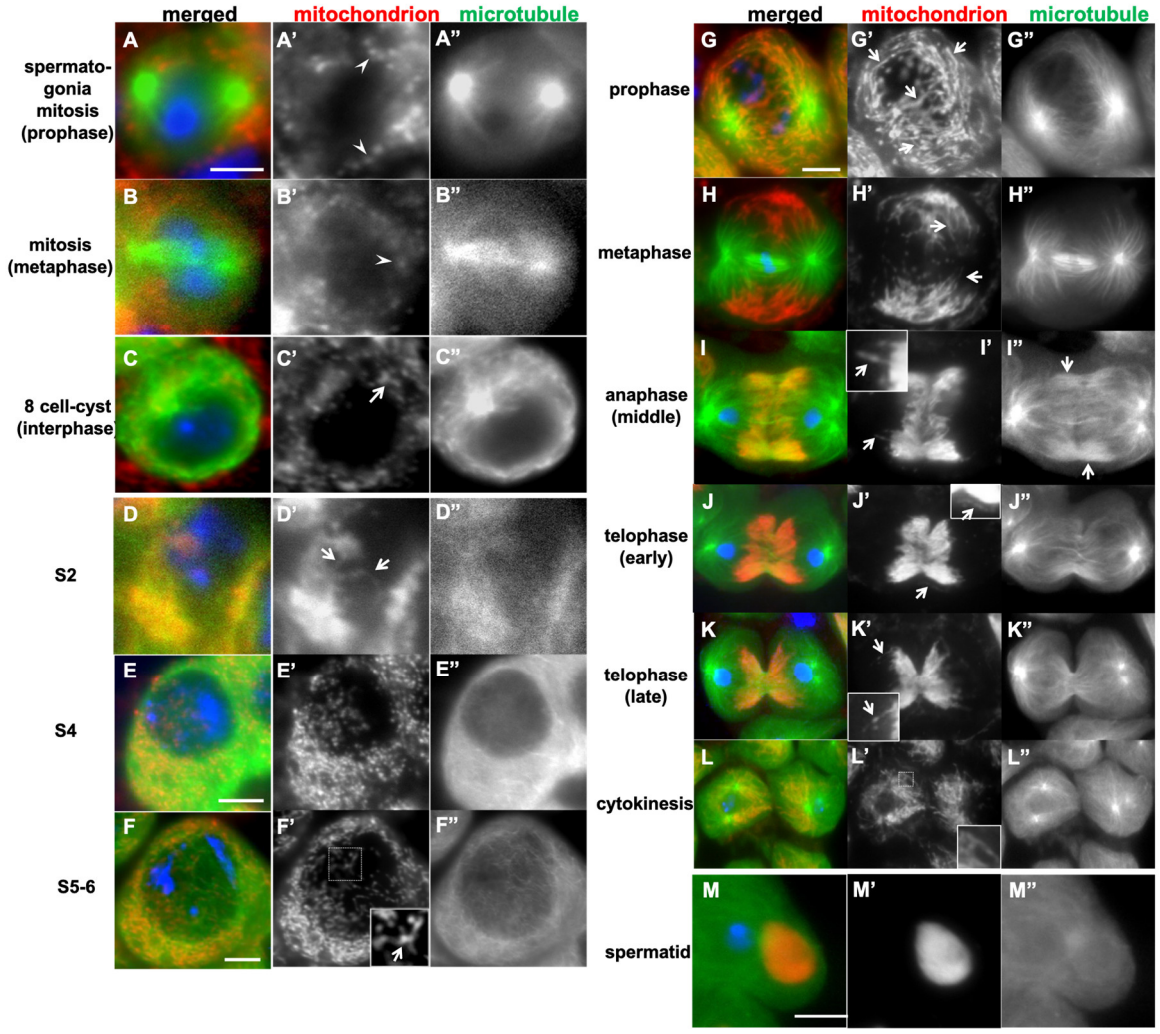

Figure 1. Differences in mitochondrial morphology between spermatogonia undergoing mitosis and spermatocytes before and during the first meiotic division in *Drosophila*. (A-H) Immunostaining of spermatogonia and spermatocytes expressing GFP-Tubulin (green in A-M, white in A''-M'') using Complex V alpha-subunit antibody (red in A-M, white in A'-M'). Blue in A-M indicates DNA. (A-C) Spermatogonia undergoing mitosis (A, B) and in interphase (C). Mitochondria exhibit a granular morphology (arrowheads) at mitosis, or slightly larger clusters (arrow) in interphase. (D-F) Spermatocytes during the cell growth phase. (D) A spermatocyte at the S2b phase, in which elongated mitochondria are formed (arrows) and clustered next to the nucleus. (E) A spermatocyte at the S4. Mitochondria undergo fission and spread within the cytoplasm. (F) A spermatocyte at the S5-6, in which the mitochondrial network structure is beginning to reform (inset: a magnified view of the region enclosed by a square in F'). (G-K) The primary spermatocytes undergoing meiotic division. (G) A prophase I cell, in which the elongated mitochondrial network structures (arrows) are maintains. (H) A

 doi:10.20944/preprints202509.0318.v1

metaphase I cell. Mitochondria accumulate near the plus ends of the aster microtubules while maintaining the elongated structure (arrows). (I, J) Anaphase I cells. Elongated mitochondria (arrows) are localized on the central spindle microtubules. From telophase I (K) to cytokinesis (L), mitochondria are equally distributed to the daughter cells from central spindle microtubules. (L) They diffuse into the cytoplasm as the midbody microtubules disintegrates. (M) Upon completion of the second meiotic division, mitochondria form single aggregate, Nebenkern. Insets in I′, K′, and L′: magnified views. Bars: 10 μm.

Next, we examined whether mitochondria maintain a membrane potential essential for ATP synthesis during meiotic divisions. We stained spermatocytes with MitoTracker, which accumulated in the mitochondrial membrane in a membrane potential-dependent manner, and performed a time-lapse observation of a living spermatocyte undergoing meiosis I. Active mitochondria stained with Mito Tracker have an active electron-transfer system and are capable of ATP synthesis. Mitochondria were distributed to daughter cells through meiosis I (Figure S2), while maintaining their ATP-synthesizing ability.

2.2. The Formation of Mitochondrial Network Structures and Their Subcellular Distribution Were Perturbed by the Inhibition of Microtubules and F-Actin

We next investigated whether the changes in mitochondrial distribution depend on microtubules or the F-actin cytoskeleton. Even after depolymerization of microtubules, mitochondria continued to be assembled next to the nucleus at the early stage (S2b) of the cell growth phase (Figure 2A), as in the untreated cells. Mitochondria were observed in the same elongated network structure (arrows in Figures 2A′ and 1D′). In the untreated cells, this network structure was constructed at the mature stage (S6) to prophase I (Figure 1F).

 doi:10.20944/preprints202509.0318.v1

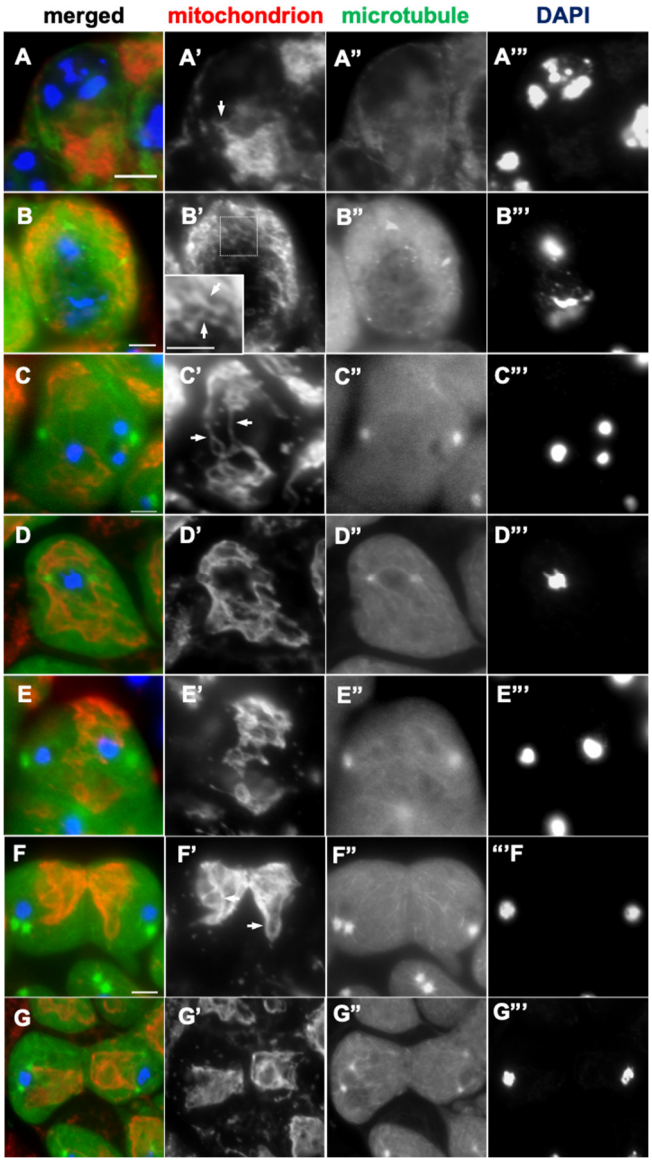

Figure 2. The distribution of mitochondria associated with microtubules in primary spermatocytes was disrupted by colchicine treatment.(A- G) Immunostaining of colchicine-treated primary spermatocytes with anti-Complex V alpha-subunit antibody to visualize mitochondria (red in A-G, white in A′-G′). The cells expressing GFP-Tubulin (green in A-G, white in A″-G″) were used to confirm the microtubule depolymerization. Blue in A-H indicates DNA. (A) A colchicine-treated spermatocyte at S2b, in which the elongated mitochondria (arrow) are maintained. (B) Spermatocytes at the S6 stage, in which the elongated mitochondria are maintained after colchicine treatment (arrows). (inset: enlarged view of the area enclosed by a square). (C-G) Mitochondria in colchicine-treated spermatocytes undergoing meiosis I at prophase-like (C) and metaphase-like (D) stages. Note that mitochondria remained localized in the cytoplasm while maintaining their network structure (arrows in C′). (E, F) Cells that have passed through metaphase I/anaphase I before colchicine treatment. Note that the alignment of mitochondria along microtubules and orientations toward the microtubule-organizing center is lost (arrows in F′). (G) Telophase I cells in which elongated mitochondrial structures are maintained between sister nuclei. Bars: 10mm.

Despite of the absence of microtubules (Figure 2B″), the similar mitochondrial structure was observed in the spermatocytes (Figure 2B′) (102 cells/176 S6-like cells), suggesting that microtubules are not essential for mitochondria to form the network structure. Despite the aster microtubules being disintegrated by colchicine treatment in the prometaphase I cells (Figure 2D″), mitochondria left the position where microtubules were present (Figure 2C′-E′), while maintaining their network structure (32 cells/50 cells). The mitochondrial structure, which was oriented toward the spindle poles before

 doi:10.20944/preprints202509.0318.v1

colchicine treatment (Figure 1I′, J′), lost its orientation after the treatment (arrows in Figure 2E, F) (35 cells/46 cells). On the other hand, the ribbon-like shape of mitochondrial structure (Figure 1J, K) was maintained in the colchicine-treated meiotic cells (Figure 2F). Mitochondria were accumulated between the separated homologous chromosomes, even if the central spindle structure was disintegrated. The mitochondria then appeared to be distributed through the cytoplasm during cytokinesis, as seen in untreated cells (Figure 2G).

Next, we examined whether F-actin is also required for mitochondrial morphology and distribution in pre-meiotic and meiotic cells. Mitochondria accumulated in the cytoplasm of the polar spermatocytes (at S2b) and Nebenkerns in spermatids at the onion stage were both co-localized with F-actin (Figure 3A and B, respectively). Thus, to examine whether the characteristic distribution of mitochondria depends on F-actin, we treated the testis cells with Latrunculin A, an inhibitor of Actin polymerization. Mitochondria were accumulated next to the nucleus at S2b, as seen in the untreated cells (Figure 3C). Some of the mitochondria were not accumulated on the cytoplasmic space next to the nucleus in the cells lacking F-actin (Figure 3C). At the S6, when the most elongated mitochondria are observed in the untreated cells, the appearance of granular mitochondria was noted after latrunculin A treatment (Figure 3D), indicating that depolymerization of F-actin inhibited the formation of the characteristic mitochondrial network structures. By contrast, the network structure, consisting of elongated mitochondria, was maintained in the meiotic cells treated with Latruncurin A (arrow in Figure 3E′), while the intracellular distribution of mitochondria was partially affected: some mitochondrial clusters were not accumulated on the equator below the cell cortex, unlike in the untreated cells. The drug-treated cells at late anaphase I (Figure 3F) and telophase I (Figure 3G) kept mitochondria on the central spindle microtubules, but not uniformly distributed (30 cells/45 cells). Therefore, we conclude that F-actin is required for the subcellular localization of mitochondria during meiosis. After Latruncurin A treatment, abnormally shaped Nebenkerns, in which mitochondria were assembled homogenously, were observed (Figure 3H) (111 cells/121 cells). F-actin is also required to produce the characteristic mitochondria morphology and distribution before and during meiosis, and additionally, for Nebenkern formation after meiosis.

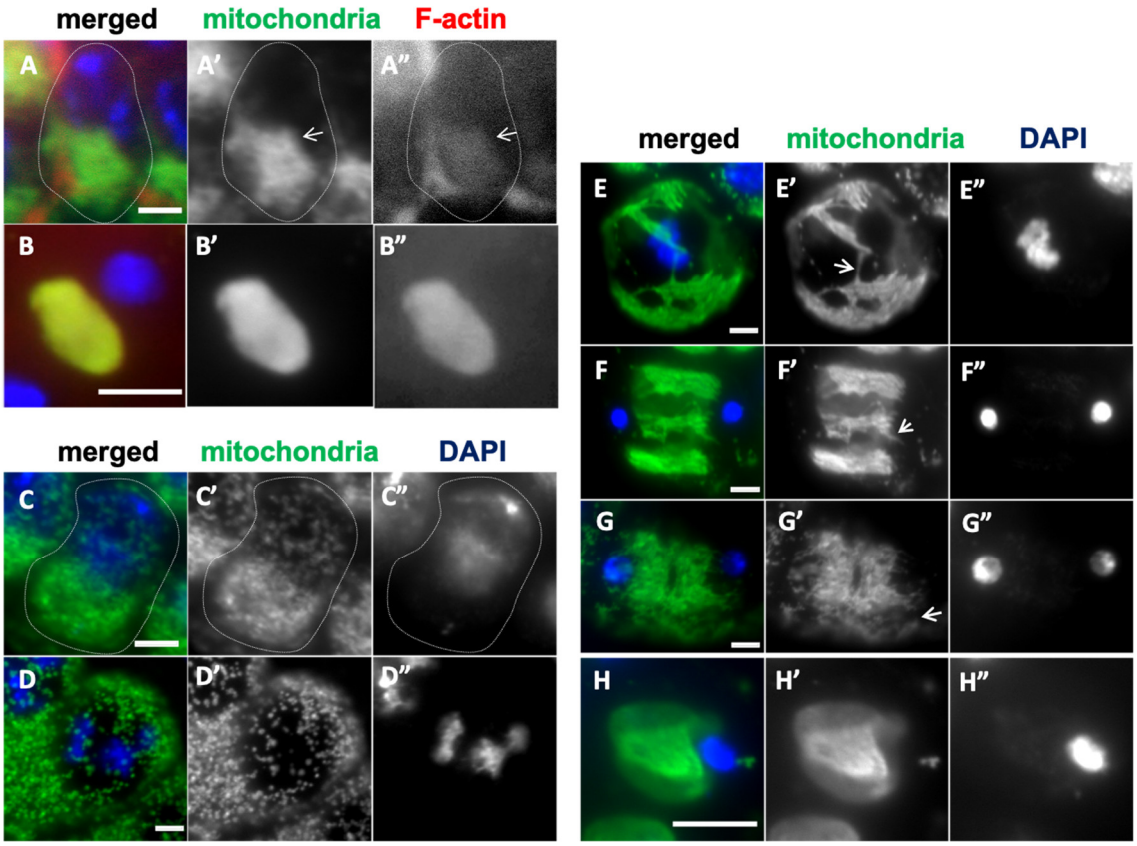

 doi:10.20944/preprints202509.0318.v1

Figure 3. A close association of the mitochondria with F-actin in spermatocytes at S2b of the growth phase and in early spermatids, and the perturbation of the distribution after Latrunculin A treatment. (A, B) Anti-Complex V alpha-subunit immunostaining to observe colocalization of mitochondria (green in A, B, white in A′, B′) with F-actin, which was visualized by phalloidin staining (red in A, B, white in A″, B″) of early spermatocytes at S2b (A) and spermatids at onion stage (B). The arrow indicates elongated mitochondria in the S2b cell. A mitochondrial aggregate (Nebenkern) colocalizes with F-actin in the spermatid (B). (C-H) Mitochondria in the cells treated with Latrunculin A were visualized by the immunostaining (green in C-H, white in C′-H′). DNA staining by DAPI (blue in C-H, white in C″-H″). (C) Mitochondria in a spermatocyte at the S2b. Note that they are not elongated, and some of them do not stay next to the nucleus. (D) Shortened granular-like mitochondria in the spermatocyte at S6. (E-H) Mitochondria in Latruncurin A-treated cells undergoing meiosis I, at metaphase I (E), anaphase I (F), telophase I (G), and Nebenkern exhibiting the heterogeneous staining in spermatids (H). Bars: 10 μm.

2.3. Formation of the Elongated Mitochondria Was Inhibited by the Knockdown of the Fusion Factors and the Mitochondrial Morphology Proteins

To investigate whether the mitochondrial fusion factors, Marf and Opa1are involved in the formation of elongated mitochondria in the spermatocytes of the cell growth phase, we observed mitochondrial morphology using confocal microscopy and super-resolution microscopy. We also examined whether the knockdown of mitochondrial morphology proteins, Letm1 and EndoB, influenced the formation of the structure. By ectopic expression of dsRNAs against *Opa1*, *Marf*, *Drp1*, and *EndoB* mRNAs in the spermatocytes, we confirmed that each mRNA was depleted by less than 10% of controls (Figure S3). In normal spermatocytes at the early stage (S2b) of the cell growth phase, mitochondria formed the elongated structure extending to 1 μm or longer, and were clustered next to the nucleus (Figure 4A). By contrast, in both *Marf*- depleted spermatocytes and *Opa1*-depleted cells, short and granule-shaped mitochondria (approx. 0.2 μm in length), dispersed through the cytoplasm without being accumulated on the cells (all of n > 160 *MarfRNAi*^{JF}, *MarfRNAi*^{GD}, and *Opa1RNAi*^{KK}) (Figure 4B′, C′). Meanwhile, when a fission factor, Drp1, was down-reg ulated by knockdown of *Drp1* (*Drp1RNAi*^{JF}) or ectopic expression of a dominant-negative mutant, *Drp1*^{DN}, in spermatocytes, these cells maintained the clustering of mitochondria at the S2b, as seen in the control. Regarding the shortened mitochondrial structure at the S3 and S4 in the control, we were unable to detect any distinct differences in the mitochondrial morphology in the cells, where Drp1 was downregulated.

As the cell growth phase progresses, mitochondria form an elongated network structure by the onset of meiosis in normal cells (Figure 4F). In contrast, small granular-shaped mitochondria were observed in all cells with knockdown of the fusion factors, *Marf* and *Opa1* (Figure 4G, H) (n > 325 cells in *MarfRNAi*^{GD} and *Opa1*RNAi^{KK}). In the S6 phase immediately before the onset of meiosis, normal cells formed elongated mitochondria with lengths exceeding 2μm (Figure 4F). In contrast, the largest spermatocytes with *Marf*-knockdown and *Opa1*-knockdown contained mitochondria in granular form with approximately 0.2 μm in length (Figure 4G, H). Furthermore, we confirmed the absence of the elongated mitochondria in the *Opa1RNAi*^{KK} cells using super-resolution microscopy (Figure S4A). Therefore, we conclude that the fusion factors, Marf and Opa1, are required for the formation of the elongated mitochondria at S2b and S6. On the other hand, the largest spermatocytes with knockdown of the fission factor, Drp1 (*Drp1RNAi*^{JF}), and those with ectopic expression of a dominant negative mutant, *Drp1*^{DN}, contained the elongated mitochondria as seen in normal cells (Figure S4B).

EndoB-depleted spermatocytes and the *Letm1*-depleted cells possessed shortened and granular-shaped mitochondria with shorter than 1 μm at the S2b and S6. The abnormally shaped mitochondria were also dispersed throughout the cytoplasm in the spermatocytes with knockdown of these factors, even at the most developed stage (Figure 4I′, J′) (all of *EndoBRNAi*^{GD} and *Letm1RNAi*^{GD} cells (n > 523 cells examined in each) (see super-resolution microscopic images in Figure S4C). These mitochondrial morphology proteins are also required for the formation of elongated mitochondria.

 doi:10.20944/preprints202509.0318.v1

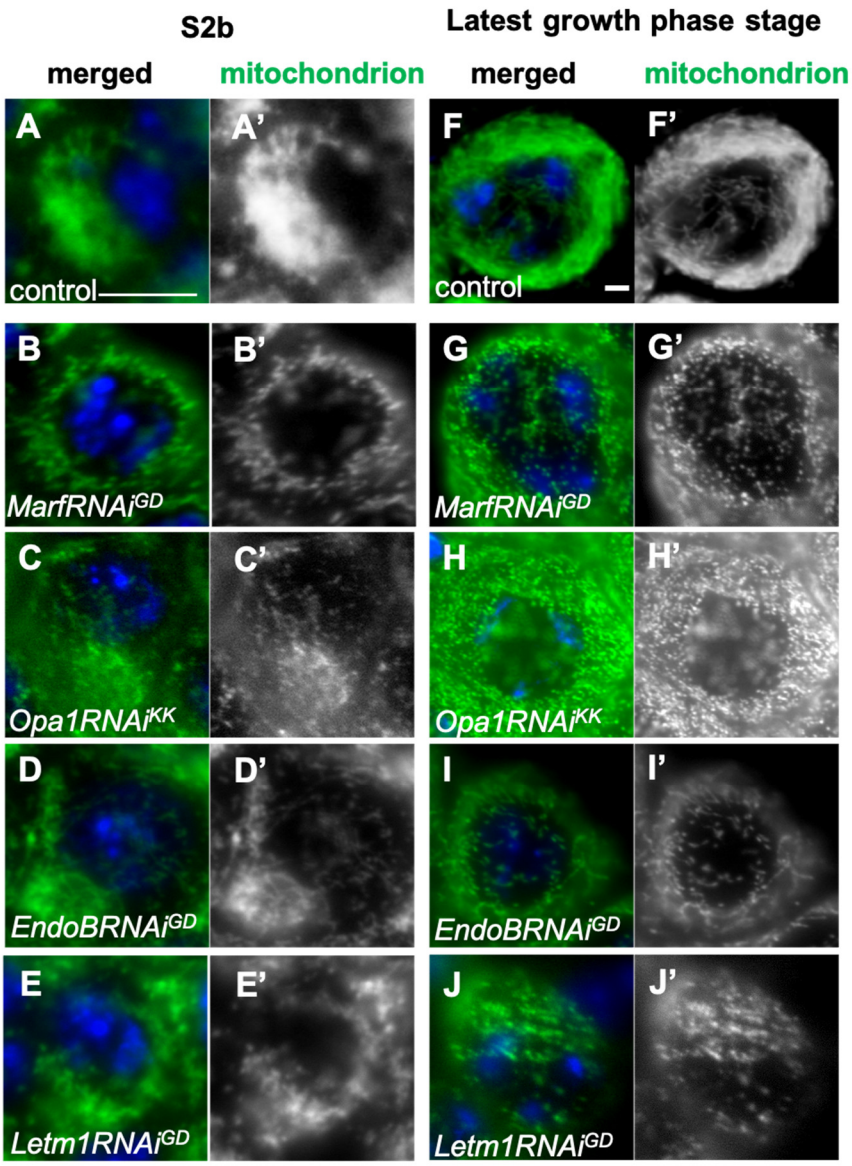

Figure 4. Knockdown of mitochondrial fusion factor genes, *Marf* and *Opa1,* and that of *EndoB* and *Letm1* encoding mitochondrial morphology proteins, and their distribution in spermatocytes during the cell growth phase. (A-J)Immunostaining of early spermatocytes at S2b (A-E), and at S6 or the most developed stages of the growth phase (F-J) to visualize mitochondria (green in A-J, white in A'-J'). Blue in A-J: DNA. (A, F) Wild-type (control) spermatocytes at S2b (A) and S6 (F). Spermatocytes at S2b (A-E) and S6 (F-J) with a knockdown of mitochondrial fusion factors, Marf and Opa1, and the morphology proteins, EndoB and Letm1. (B, G) *MarfRNAi*^{GD}, (C, H) *Opa1RNAi Opa1RNAi*^{KK}. Spermatocytes at S2b (D, E) and S6 (I, J) with a knockdown of *EndoB* and *Letm1*. (D, I) *EndoBRNAi*^{GD}. (E, J) *Letm1RNAi*^{GD}. Bars: 10mm.

2.4. Knockdown of the Fusion Factors and the Morphology Proteins Inhibited ATP Synthesis and Cell Growth in the Spermatocytes Before Meiosis

As the formation of elongated mitochondria, which retain increased ATP synthesis capabilities, was affected by the knockdown of fusion factors and morphology proteins, we examined whether ATP levels decreased in those testes. The average ATP amount in control testes was 65.6 ± 8.4 mmol/mg. By contrast, when *blw*, encoding the mitochondrial ATP synthase alpha-subunit, was depleted in the testis cells, the mean ATP amount decreased by 7.9 ± 0.3 mmol/mg. Thus, we next quantified ATP amounts in the testes with knockdown of *Marf, Opa1, EndoB, and Letm1*. Those in the testes with knockdown of the mitochondrial fusion factors decreased up to 45% of the control, as

 doi:10.20944/preprints202509.0318.v1

follows: 30.9 ± 0.7 mmol/mg in *MarfRNAi*^{JF}, 35.9 ± 0.5 mmol/mg in *MarfRNAi*^{GD}, 29.2 ± 0.4 mmol/mg in *Opa1RNAi*^{HMS}, and 31.2 ± 0.5 mmol/mg in *Opa1RNAi*^{KK}. Consistently, the mean levels in testes with knockdown of the morphology proteins also decreased as follows: 6.2 ± 0.3 mmol/mg in *EndoBRNAi*^{KK}, and 7.0 ± 0.3 mmol/mg in *EndoBRNAi*^{GD}, 10.5 ± 0.2 mmol/mg in *Letm1RNAi*^{GD}, and 10.4 ± 0.6 mmol/mg in *Letm1RNAi*^{HMS}. These data suggest that ATP synthesis in mitochondria was reduced due to the knockdown of mitochondrial fusion factors and the morphology proteins.

2.5. The Cell Growth Before Male Meiosis Was Affected in the Spermatocytes with the Knockdown of Mitochondrial Fusion Factors and the Morphology Proteins

The average diameter of most developed spermatocytes with *blw*-knockdown was 27.0 ± 0.3μm (the bottom of Figure 5). It was considerably smaller than that in control spermatocytes at S6 (average 38.1 ± 0.3μm) (the top of Figure 5). Thus, we investigated whether the reduced ATP levels in the spermatocytes with knockdown of the mitochondrial fusion factors and the morphology proteins resulted in inhibition of the cell growth before meiosis. In contrast to the remarkable cell growth in normal spermatocytes, the maximum diameter was 30.3 ± 0.2μm in spermatocytes from the *sa* mutants, where the progression of cell growth is arrested in the middle of the growth phase. Similarly, it was 32.2 ± 0.3μm in *twe* mutants, where the meiotic cell cycle is arrested just before the onset of meiosis. Next, we measured the cell diameter of the most developed spermatocytes with the knockdown of the fusion factors and the morphology proteins. The average diameters of spermatocytes with knockdown of the fusion factors at the most developed stage were as follows: 29.7 ± 0.4μm for *MarfRNAi*^{JF}, 29.6 ± 0.2μm in *MarfRNAi*^{GD}, 31.6 ± 0.3μm in *Opa1RNAi*^{HMS}, and 29.8 ± 0.4μm in *Opa1RNAi*^{KK}. The average diameters of these knockdown cells were as small as that of the *sa* mutant cells. Consistently, *Letm1*-depleted spermatocytes at the most developed stage (23.7 ± 0.2μm for *Letm1*RNAi^{HMS}, and 23.6 ± 0.7μm for *Letm1RNAi*^{GD}) were significantly smaller than normal spermatocytes at S6. Knockdown of mitochondrial fusion factors, Marf and Opa1, and the morphology proteins, EndoB and Letm1, affected the cell growth of spermatocytes before male meiosis.

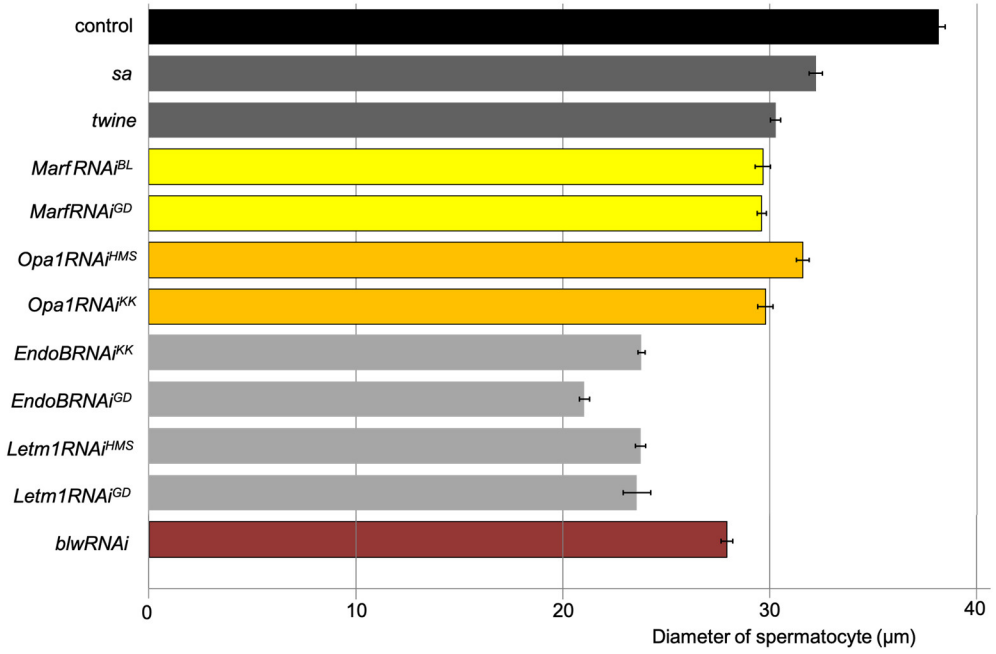

Figure 5. Growth inhibition of spermatocytes with knockdown of mitochondrial fusion factors, the morphology proteins, and the *blw* gene encoding the mitochondrial complex V α subunit. The horizontal axis shows the mean diameter (μm) of the control spermatocytes at S6 stage, those of the cells at the most developed stages with knockdown of mitochondrial fusion factor genes, *Marf* (yellow: *MarfRNAi*^{JF} and *MarfRNAi*^{GD}) and *Opa1*(orange:

 doi:10.20944/preprints202509.0318.v1

Opa1RNAi^{HMS} and *Opa1RNAi*^{KK}), the cells with knockdown of mitochondrial morphology genes, *EndoB* (gray: *EndoBRNAi*^{KK} and *EndoBRNAi*^{GD}) and *Letm1*(gray: *Letm1RNAi*^{HMS} and *Letm1RNAi*^{GD}), and the cells with knockdown of *blw* (brown: *blwRNAi*). The diameters of spermatocytes within the cysts at the S6 or the most developed stages (n ≥ 20 cells) were measured, and the average length is shown on the horizontal axis. The largest cells with knockdown of mitochondrial fusion and fission factors have significantly smaller diameters than control cells. $p < 0.0001$ in every genotype compared with control (Student's *t*-test). Error bars indicate the standard error of the mean.

2.6. The Phenotype Observed in Spermatids when Chromosome Separation During Meiosis Is Abnormal Was Caused by Knockdown of Mitochondrial Fusion and Fission Factors, and Morphogenesis Proteins

While the *blw*-knockdown inhibited cell growth of the spermatocytes, the knockdown cells completed both meiotic divisions and formed the normal-looking cysts consisting of 64 spermatids. Thus, we next investigated whether the knockdown of mitochondrial fusion and fission factors affected the execution of meiosis. Sixteen pre-meiotic spermatocytes undergo two rounds of meiotic divisions synchronously. Consequently, 64 spermatocytes containing single nuclei of the same size are produced in normal testes (Figure 6A). In contrast, 20% of single intact cysts of spermatids derived from *Marf*-depleted spermatocytes (*MarfRNAi*^{GD}) were composed of 33 to 63 cells (Figure 6B, Table 1). Consistently, all of the intact spermatid cysts from spermatocytes with knockdown of another fusion factor, *Opa1* (*Opa1RNAi*^{HMS}), contained only 16 cells. 15% of the intact cysts were composed of 16 to 31 cells among the spermatid cysts that differentiated from *Opa1*RNAi^{KK} spermatocytes (Figure 6C, Table 1). These phenotypes resembled those of the *twe* mutant males, where spermatocytes differentiate without one or both meiotic divisions. Although spermatids derived from *Drp1*-depleted spermatocytes (*Drp1RNAi*^{JF}) formed cysts made up of 64 normal looking cells (all in 59 cysts examined) (Table 1), 60% of the intact cysts were consisted of 33–63 cells, fewer than 64 cells among intact spermatid cysts derived of spermatocytes expressing a dominant-negative mutant for *Drp1*, *Drp1*^{DN} (30 cysts/51 cysts examined)(Figure 6D, Table 1). These results suggest that meiosis was not correctly completed in some of these spermatocyte cysts. Consistent with the knockdown of the fusion and fission factors, 90% of spermatid cysts from *EndoB*-depleted spermatocytes and all spermatid cysts from *Letm1*-depleted spermatocytes consisted of only 16 cells (Figure 6E, G, Table 1), suggesting that both meiotic divisions did not take place in the *EndoB*- and *Letm1*-depleted spermatocytes. In summary, knocking down mitochondrial fusion and fission factors, along with morphology proteins, in spermatocytes impacted male meiosis.

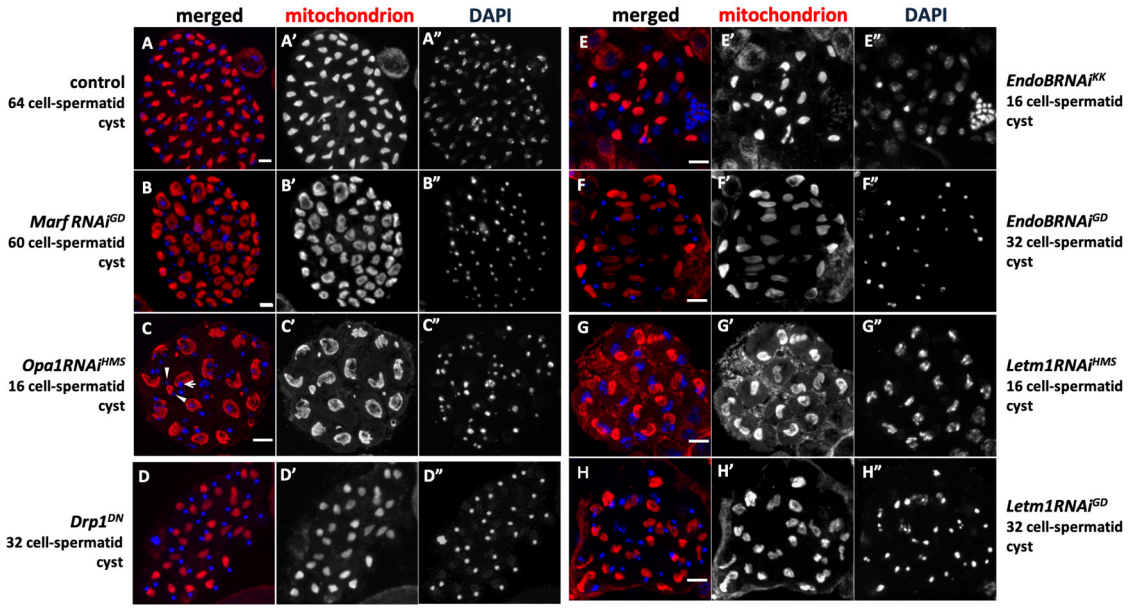

 doi:10.20944/preprints202509.0318.v1

Figure 6. Abnormal spermatid cysts derived from the spermatocytes with knockdown of mitochondrial fusion and fission factors, and EndoB and Letm1 without undergoing either one or both of meiotic divisions. (A-H) Immunostaining to visualize mitochondria (red in A-H, white in A'-H') in the spermatids of intact cysts at the onion stage. Blue in A-H, white in A"-H"; DNA staining. (A) An intact cyst composed of 64 spermatids in control testis, in which was produced via two meiotic divisions. (B-D) Intact spermatid cysts derived from spermatocytes with a knockdown of mitochondrial fusion factor genes, *Marf* (B; *MarfRNAi*^{GD}) and *Opa1* (C; *Opa1RNAi*^{GD}, D; *Opa1RNAi*^{HMS}). (B) An intact spermatid cyst composed of 60 cells in *MarfRNAi*^{GD} testis. (C) An intact cyst composed of only 16 cells in *Opa1RNAi*^{HMS} testis. An arrow in C indicates an example of nuclei with normal size, and arrowheads indicate smaller nuclei. (D) An intact cyst composed of only 32 cells in the testis expressing a dominant negative mutant for a fission gene, *Drp1*^{DN}. (E-H) Intact spermatid cysts derived from spermatocytes with knockdown of mitochondrial membrane protein genes, *EndoB* (E; *EndoBRNAi*^{KK}, F; *EndoBRNAi*^{GD}) and *Letm1* (G; *Letm1RNAi*^{HMS}, H; *Letm1RNAi*^{GD}). (E) An intact cyst composed of only 16 cells in *EndoBRNAi*^{HMS} testis, (F) an intact cyst composed of only 32 cells in *EndoBRNAi*^{GD} testis, (G), an intact cyst composed of only 16 cells in *Letm1RNAi*^{HMS} testis, (H) an intact cyst composed of only 32 cells in *Letm1RNAi*^{KK} testis. Bars: 10 mm.

Table 1. Frequencies of abnormal spermatid cysts, which resulted from meiotic defects in spermatocytes with depletion of mitochondrial fusion and fission factors and the morphology proteins.

Knockdown & Dominant negative exp.	16 cell-cysts*	17-31 cell-cysts	32 cell-cysts	33-63 cell-cysts	64 cell-cysts(normal)
control	0(0)	0(0)	0(0)	0(0)	68(100)
MarfRNAi^{JF}	0(0)	0(0)	0(0)	0(0)	50(100)
MarfRNAi^{GD}	0(0)	0(0)	0(0)	8(20.0)	32(80.0)
Opa1RNAi^{HMS}	3(3.2)	0(0)	2(2.2)	0(0)	88(94.6)
Opa1RNAi^{KK}	97(84.3)	16(15.7)	0(0)	0(0)	0(0)
Drp1RNAi^{JF}	0(0)	0(0)	0(0)	0(0)	59(100)
Drp1^{DN}	0(0)	0(0)	0(0)	30(58.8)	21(41.2)
EndoBRNAi^{KK}	54(100)	0(0)	0(0)	0(0)	0(0)
EndoBRNAi^{GD}	42(82.4)	0(0)	9(17.6)	0(0)	0(0)
Letm1RNAi^{HMS}	40(100)	0(0)	0(0)	0(0)	0(0)
Letm1RNAi^{GD}	42(84.0)	0(0)	8(16.0)	0(0)	0(0)

The numbers of intact spermatid cysts (%) observed in the testes with each genotype (n>50 cysts were examined).* Intact spermatid cysts composed of the number of cells indicated there.

Furthermore, in testes lacking mRNA for mitochondrial fusion factors, cysts containing abnormal spermatids resulting from failed chromosome segregation in meiosis were observed. The spermatids derived from the spermatocytes of *MarfRNAi*^{GD}, *Opa1RNAi*^{HMS,} and *Opa1RNAi*^{KK} contained two or more nuclei, which were smaller than the nuclei of normal spermatids (e.g., arrowheads in Figure 6C). The nuclei of the *Opa1RNAi*^{HMS} and *Opa1RNAi*^{KK} cells were often different in size among spermatids within the same cysts (72.9% and 30.0%, respectively) (e.g., arrows and arrowheads in Figure 6C', Table 2). These phenotypes occur when chromosome segregation is arrested prematurely, resulting in the formation of small nuclei on lagging chromosomes.

 doi:10.20944/preprints202509.0318.v1

Table 2. Frequencies of spermatid cysts with abnormal nuclear numbers and size, which were generated from abnormalities in meiotic divisions, which were derived from spermatocytes harboring a depletion of *opa1*.

Knockdown	n	nuclear numbers in a spermatid (%)							macro/ micro nuclei (% cells)
		normal	abnormal						
		1	0	2	3	4	5>	Total (%)	
control	1,290	99.5	0.4	0.1	0	0	0	0.5	0
Opa1RNAi^{HMS}	1,713	27.1	7	24.3	15.8	12.3	13.4	73.9	23.5
Opa1RNAi^{KK}	952	70	29.9	12.2	11.6	4.6	1.5	30	32.4

2.7. Knockdown of Mitochondrial Fusion Factors Inhibited Cdk1 Activation in the Primary Spermatocytes Before the Onset of Meiosis

The entry to the M-phase is controlled by the activation of a cyclin-dependent kinase, Cdk1. To determine why meiotic divisions failed in spermatocytes with knockdown of mitochondrial fusion factors, we investigated Cdk1 activation (Figure 7). The MPM-2 antibody recognizes the amino acid sequences phosphorylated by Cdk1 (p-Ser/p-Thr-Pro). Anti-MPM-2 immunostaining of normal spermatocytes at the mature stage (S6) showed intense signals in the nucleolus within the nucleus (arrow in Figure 7A), corresponding to a phosphorylation of nucleolar proteins by Cdk1. In contrast, among the largest spermatocytes with knockdown of mitochondrial fusion factors, Marf and Opa1, few cells exhibiting strong immunostaining signals on the nucleolus were observed (Figure 7B-E). In some *Opa1*-depleted spermatocytes, we observed multiple small dot-like signals within the nucleus (Figure 7D', E'). However, these were not as prominent as the signals seen in control cells. Consistently, in *EndoB*- and *Letm1*-depleted spermatocytes, MPM-2 punctate signals were observed in a less prominent form at locations that did not correspond to nucleoli (Figure 7F, G). However, we observed similar MPM2 signals in the control cells, even in the largest spermatocytes with the *Drp1* knockdown (*Drp1RNAi*^{IF}) or expressing the dominant-negative mutant, *Drp1*^{DN} (>100 cells/>10 cysts examined). The above observations suggest that Cdk1 was not fully activated in the premeiotic cells, where mitochondrial fusion and fission factors, and EndoB and Letm1, were depleted, consistent with the conclusions inferred from the meiotic phenotype that appeared in the resultant spermatid cysts premeiotic

 doi:10.20944/preprints202509.0318.v1

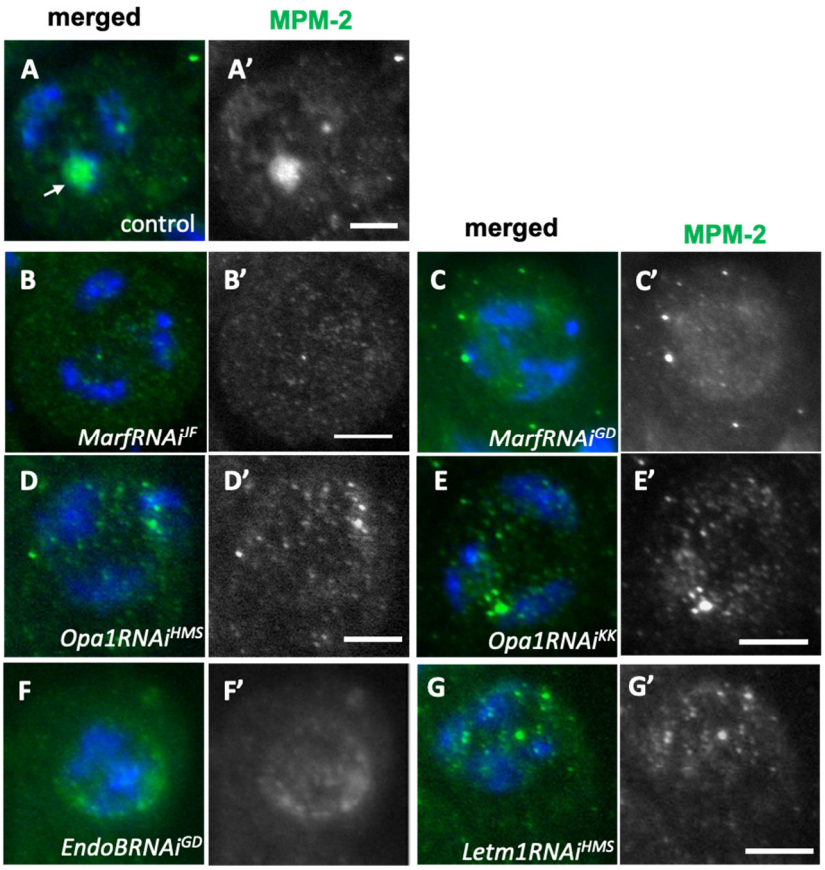

Figure 7. Absence of activated Cyclin-dependent kinases in spermatocytes with knockdown of mitochondrial fusion and fission factors. (A-G) Immunostaining of spermatocytes with MPM2 antibody that recognizes proteins phosphorylated by the activated CDK1. (A) In wild-type spermatogonia before the onset of meiosis, a strong anti-MPM2 signal is observed on the nucleolus (arrow). (B-G) The spermatocytes with knockdown of mitochondrial fusion factors, Marf (B: *MarfRNAi*^{JF}, C: *MarfRNAi*^{GD}) and Opa1(D: *Opa1RNAi*^{HMS}, E: *Opa1RNAi*^{KK}). Note that the strong anti-MPM2 signals are not observed in the knockdown cells. (F, G) The spermatogonia with knockdown of the mitochondrial morphology factors, EndoB (F: *EndoRNAi*^{GD}) and Letm1(G: *Letm1RNAi*^{HMS}). Dot-like immunostaining foci do not colocalize with the nucleolus. Blue in A-G: DNA. Bars: 10mm.

2.8. Inhibition of Meiotic Initiation Caused by Knockdown of Mitochondrial Fusion Factors and the Morphology Proteins Was Partially Rescued by Ectopic Overexpression of Cyclin B

Next, we addressed a mechanism by which the knockdown of mitochondrial fusion factors resulted in the inhibition of Cdk1 activation. The activation of the kinase is regulated by the expression and intracellular localization of Cyclin B (CycB). This M-phase cyclin is barely expressed at the middle stage (S4) in the growth phase of spermatocytes (Figure 8A). Intense CycB signals were observed in both the cytoplasm and nucleus by the end of the growth phase (S6), which occurs before meiosis begins (Figure 8A'). In contrast, in spermatocytes with knockdown of *Opa1* and *Marf* (*Opa1RNAi*^{HMS} and *MarfRNAi*^{GD}), no spermatocytes with distinct CycB accumulation were found (>80 cells (>5 cysts) were examined) among the largest spermatocytes (Figure 8C', D'). Similarly, in spermatocytes where *EndoB* and *Letm1* was depleted, no spermatocytes with a distinct CycB accumulation were found (Figure 8E', F'). However, we have not found significant changes in CycB accumulation in the cytoplasm and/or nucleus even in the largest spermatocytes with the *Drp1* knockdown (*Drp1RNAi*^{JF}) or expression of a dominant-negative mutant (*Drp1*^{DN}) (>100 cells (>10 cysts) were examined). These results are consistent with the finding that no cells harboring active Cdk1 were observed in the testes, where mitochondrial fusion factors and the morphology proteins were depleted.

Preprints.org (www.preprints.org) | NOT PEER-REVIEWED | Posted: 3 September 2025 doi:10.20944/preprints202509.0318.v1

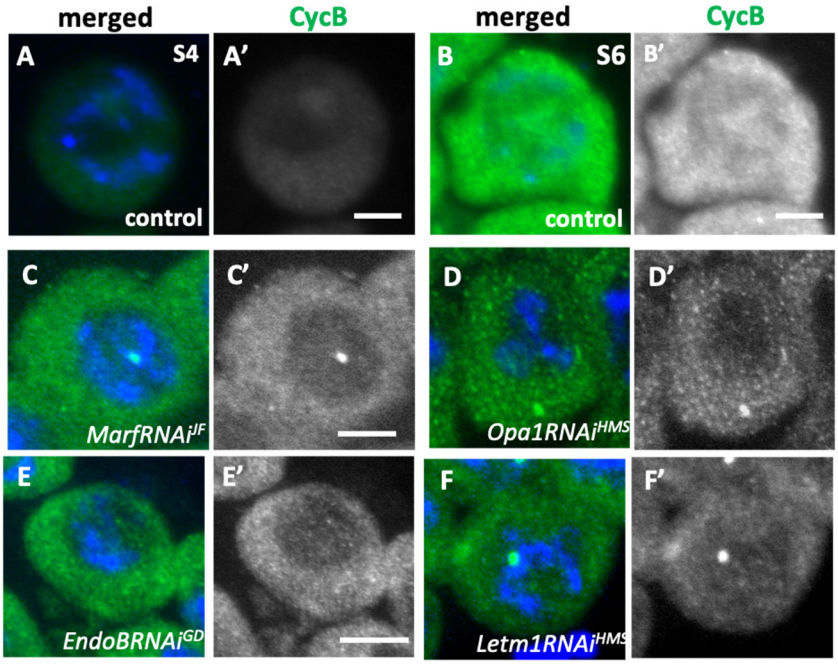

Figure 8. A loss of Cyclin B accumulation in the nuclei of spermatocytes harboring a knockdown of mitochondrial fusion factors and the morphology proteins. (A-F)Anti-Cyclin B (CycB) immunostaining of primary spermatocytes (green in A-F, white in A'-F'). Blue in A-F: DNA. (A, B)The immunostaining signals in wild-type spermatocytes at mid-cell growth phase (the S4 stage)(A), and the S6 (B), in which the robust CycB signal was accumulated in the cytoplasm as well as in the nucleus. (C-F) The spermatocytes with knockdown of mitochondrial fusion factors, Marf (C: *MarfRNAi*^{JF},) and Opa1(D: *Opa1RNAi*^{HMS}), and those with that of the mitochondrial morphology proteins, EndoB (E: *EndoBRNAi*^{GD}) and Letm1(F: *Letm1RNAi*^{HMS}) at the most developed stages. Note that the CycB accumulation was less than that in the wild type, and no cells harboring its accumulation in the nucleus were observed. Bars: 10mm.

To investigate whether a failure of meiotic initiation in the spermatocytes with knockdown of mitochondrial fusion factor was due to the reduced CycB expression, we induced the ectopic overexpression of CycB in the cells and examined whether this rescued a failure of meiosis (Table 3). As a negative control, the expression of *mCherry* led to the formation of 16-cell spermatid cysts at a high rate (84.3% among 108 cysts), but no 64-cell cysts were observed in the testes with *Opa1*-knockdown. In contrast, when *CycB* expression was simultaneously induced, the frequency of 16-cell cysts decreased (51.9% among 129 cysts), and instead, 64-cell cysts were observed (18.0 % among 129 cysts). Consistently, spermatocytes with *EndoB* knockdown and *mCherry* expression formed 16-cell spermatid cysts at a high frequency (62.6 % among 107 cysts examined), but no 64-cell cysts. In contrast, when *CycB* expression was simultaneously induced, the frequency of 16-cell cysts decreased (7.6 % among 107 cysts), and instead 64-cell cysts appeared (27.6 % among 105 cysts). Therefore, we conclude that the failure of meiosis caused by the knockdown of *Opa1* or *EndoB* was partially restored by the CycB overexpression.

Table 3. A partial rescue of the failure of meiotic divisions by the knockdown of mitochondrial fusion factor gene, *opa1*, and the morphology gene, *EndoB*, by overexpression of Cyclin B (CycB).

Knockdown & ectopic expression	16 cell-cysts (%)*1	17~31 cell -cysts	32 cell -cysts*2	33-63 cell -cysts	64 cell -cysts*3	Total cysts
Opa1RNAi^{KK}, *mCherry*	91(84.3)	16(14.8)	1(0.9)	0(0)	0(0)	108
Opa1RNAi^{KK}, *CycB*	67(51.9)	7(5.4)	33(25.6)	4(3.1)	18(14.0)	129
EendoBRNAi^{KK}, *mCherry*	67(62.6)	26(24.3)	3(2.8)	11(10.3)	0(0)	107
EndoBRNAi^{KK}, *CycB*	8(7.6)	17(16.2)	11(10.5)	40(38.1)	29(27.6)	105
CycB	0(0)	0(0)	0(0)	0(0)	106(100)	106

 doi:10.20944/preprints202509.0318.v1

*1 The number of spermatid cysts consisting of 16 cells (%), indicating that the cysts were generated from spermatocytes without any meiotic divisions.*2 The number of spermatid cysts consisting of 32 cells (%), indicating that the cysts were generated from spermatocytes via only one of either meiotic division.*3 The number of spermatid cysts consisting of 64 cells (%), indicating that the cysts were generated from spermatocytes via meiotic division I and II.

2.9. Knockdown of Mitochondrial Fusion and Fission Factors Caused Abnormalities in Nebenkern Formation in Early Spermatids After the Second Meiosis

Mitochondria assemble into a single spherical structure called a Nebenkern after meiosis completes in normal spermatid (Figure 9A). In contrast, we found incomplete Nebenkerns that failed to form a sphere in the spermatids that developed from the spermatocytes with knockdown of *Marf* (*MarfRNAi*^{GD})(Figure 9B), and *Opa1*(*Opa1RNAi*^{HMS}, *Opa1RNAi*^{KK}) (Figure 9C, D). Immunostaining of spermatids to visualize mitochondria showed that most of the Nebenkerns exhibited uneven staining, with areas in the center remaining unstained or less stained (Figure 9 B-E). (all of *MarfRNAi*^{GD} spermatids (n>325 examined), and more than 70 % of *Opa1RNAi*^{HMS} and *Opa1RNAi*^{KK} (n>952 cells). Despite being less frequent, a similar phenotype in Nebenkern morphology was also observed in spermatids expressing *Drp1*^{DN} (Figure 9E). Among spermatids in which *EndoB* or *Letm1*was depleted, more severe Nebenkern phenotypes, such as multiple smaller Nebenkerns per spermatid (arrows in Figure 9C, F, G) and unassembled mitochondria that were not integrated into a Nebenkern in the cytoplasm (Figure 6H'), were frequently observed in the spermatids. These observations suggest that the Nebenkern formation was affected by the knockdown of mitochondrial fusion and fission factors, and by that of EndoB and Letm1 (Figure 9F-I).

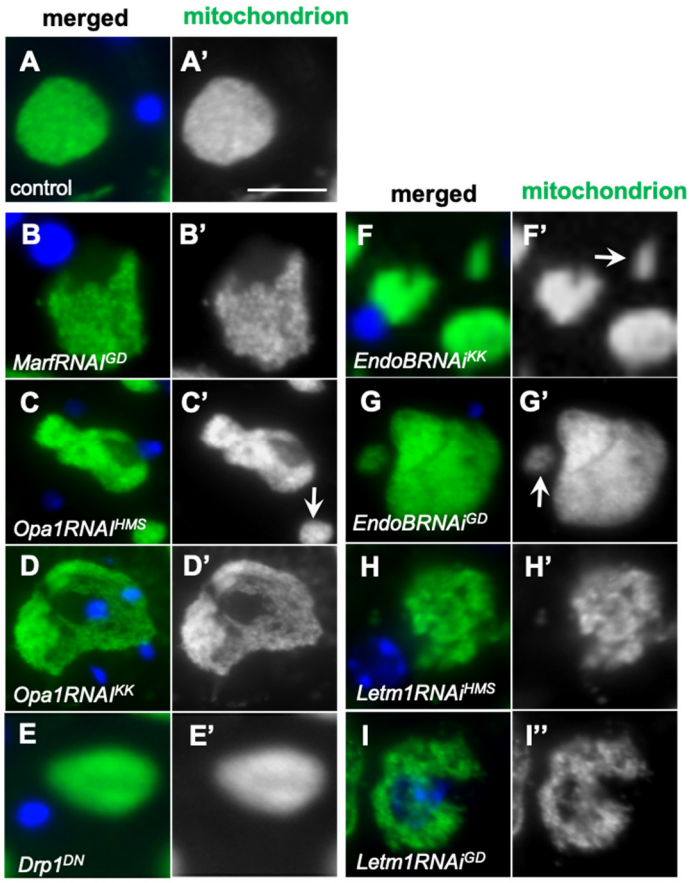

Figure 9. Abnormal formation of Nebenkerns in spermatids derived from spermatocytes with knockdown of mitochondrial fusion factors, and the morphology proteins, and those from spermatocytes expressing *Drp1*^{DN}. (A-I) Immunostaining of spermatids at the onion stage to visualize mitochondria (green in A-I, white in A'-I').

 doi:10.20944/preprints202509.0318.v1

Blue in A-I: DNA staining. (A) Control spermatid. (B-D) spermatids derived from spermatocytes with a knockdown of mitochondrial fusion factors, Marf (B; *MarfRNAi*^{GD}), and Opa1 (C; *Opa1RNAi*^{HMS} and D; *Opa1RNAi*^{KK})). (E) A spermatid from a spermatocyte expressing the dominant negative mutant (*Drp1*^{DN}). (F-I) Spermatids derived from spermatocytes with knockdown of mitochondrial morphology proteins, EndoB (F; *EndoRNAi*^{lF} and G; *EndoBRNAi*^{GD}), and Letm1 (H: *Letm1RNAi*^{HMS} and I: *Letm1RNAi*^{GD}). Note that Nebenkerns in B-I failed to be assembled into single spherical structures, and the spermatids possess multiple small Nebenkerns (arrows in C′, F′, G′). Bar: 10 μm.

3. Discussion

3.1. Mitochondria in Drosophila Spermatocytes Undergo Stage-Specific Changes Between a Shortened Form and an Interconnected Network Structure

Several studies have reported that mitochondria undergo a remarkable morphological change to form a large cluster called Nebenkern after meiosis (Fuller, 1993; Inoue et al., 2012; Vedelek et al., 2024). We focused on the investigation of mitochondrial fine structures in spermatogonia and spermatocytes before and during meiosis using high-resolution confocal microscopy, super-resolution microscopy, N-SIM, and TEM. Spermatogonia derived from germline stem cells undergo four mitotic divisions, during which shortened and granular mitochondria were observed. This morphology is consistent with that observed in mammalian cells in mitosis (Taguchi et al., 2007; Madan et al., 2022). On the other hand, we found that the mitochondrial network structure composed of elongated mitochondria and a shortened form are repeated during the development of spermatocytes. In the S2b stage corresponding to polar spermatocytes, mitochondria accumulate next to the nucleus (Cenci et al., 1994). Illustrations based on the past EM observations show discrete mitochondria in a granular shape or oval capsules that look like two fused (Tate's TEM observation in Fuller 1993). Previous observation under light microscopy also described that phase-dark structures possibly corresponding to mitochondria form clusters at this stage (Hales and Fuller, 1997; Aldridge et al., 2007). We have performed immunostaining to identify mitochondria in meiotic cells (Ichihara et al., 2007; Inoue et al., 2012). Here, we demonstrated that the network structure made of elongated mitochondria was constructed at the S2b stage and transformed into shortened forms by the subsequent apolar stages corresponding to the S3 stage. These observations are consistent with a previous description (Fuller, 1993). By the end of the growth phase, just before meiosis, the network structures were constructed. In Tate's illustration based on his EM observation, an elongated mitochondria-like structure was drawn (Fuller 1993). The metaphase I to telophase I cells have rod-shaped mitochondria whose length is more than 10 times their diameter (Fuller 1993). Our observations clarify that mitochondria form a network, which may be interconnected with multiple mitochondria before and during male meiosis. In combination with previous immunostaining results (Ichihara et al., 2007), we conclude that the organelles are associated with microtubule and nuclear envelope structures that form specifically during meiosis. They are subsequently released into the cytoplasm upon cytokinesis. This specific pattern of mitochondrial distribution suggests that a regulatory mechanism ensuring the equal segregation of mitochondria transferred to daughter cells during meiosis, rather than being the result of equal partitioning of the cytoplasm, may be present.

In mammalian cell mitosis, the mitochondrial membrane potential changes during cell division. Mitochondria are polarized until metaphase as much as in interphase cells, but thereafter, they become depolarized. After cytokinesis, the potential was recovered. The electron supply to the mitochondrial electron transfer chain is suppressed during M phase, possibly to reduce the reactive oxygen species (ROS) generated by mitochondrial fragmentation during the M phase (Hirusaki et al., 2017; Madan et al., 2022). In contrast, in Drosophila male meiosis, mitochondria maintain the network structure formed during the cell growth phase. Since active mitochondria are transferred to daughter cells while staying intact, ATP production continues uninterrupted. This may give an advantage in meiosis, as ATP supply can be provided immediately on-site. ATP is also required for morphological changes in mitochondria after the completion of meiosis II (Aldridge et al., 2007).

 doi:10.20944/preprints202509.0318.v1

3.2. Requirement of Fusion Factors for the Formation of the Mitochondrial Network, and Microtubules and F-Actin for Their Distribution Before and During Male Meiosis

This study demonstrated that Marf, which is required for the fusion of the mitochondrial outer membrane, and Opa1, for the inner membrane fusion, are indispensable for the formation of elongated mitochondrial structures at S2b and S6 stages. This is consistent with the observation in Drosophila axons and heart tubes (Westermann, 2008; Trevisan et al., 2018). When the fusion/fission balance shifts toward fission due to a decrease in fusion, the network converts a higher number of smaller mitochondria in neurons (Trevisan et al., 2018; Jones and Naylor, 2022), because Drp1 counteracts with Marf and Opa1 (Westermann, 2008). When the fission factor, Drp1, was depleted using Drp1RNAi stock that enables effective knockdown, or when $Drp1^{DN}$ was ectopically expressed, no cells with remaining elongated mitochondrial structures were observed in the subsequent stages, where the elongated structure transforms into the shortened forms. Aldridge and colleagues reported that the phase-dark structures corresponding to mitochondria form a tight cluster in the spermatocytes homozygous for the lethal allele of Drp1 at the stage (Aldridge et al., 2007). The cells with Drp1RNAi and expression of $Drp1^{DN}$ may have retained more of the normal Drp1 than spermatocytes homozygous for the lethal mutation. The mitochondrial network structure is typical of normal cells before meiosis, so even if the cluster increases in cells with lower Drp1 activity, it may be challenging to find.

In addition to the well-known GTPases as mitochondrial dynamics factors, knockdown of EndoB, which is localized to the outer membrane (OMM), and Letm1 to the inner membrane affected the formation of the mitochondrial network. In mammalian cultured cells, inhibiting EndoB1 results in an abnormal structure where only the OMM elongates (Karbowski et al., 2004). Similarly, the mitochondrial morphology and cristae structures were disturbed in the Letm1RNAi mammalian cells (Nakamura et al., 2020). These two mitochondrial morphology proteins are also required for the formation of the mitochondrial network before meiosis in Drosophila.

On the other hand, regarding the roles of cytoskeletons for the mitochondrial morphological changes, it remains to be concluded in mammalian cells as conflicting results have been reported (Ishihara et al., 2003; Mattenberger et al., 2003; Jourdain et al., 2009; Cho et al., 2021; Jones and Naylor, 2022). Although mitochondria change their subcellular distribution along microtubules, we have not observed distinct morphological alterations in mitochondria elongation and network formation after microtubule depolymerization. However, we cannot rule out that there was not enough time for detectable morphological changes in mitochondria to occur. By contrast, F-actin may play a more critical role in maintaining the mitochondrial network structure. Further experiments are needed to verify the hypothesis.

3.3. Requirement of the Mitochondrial Network Formed via the Fusion Factors for the Cell Growth of Spermatocytes Before Meiosis

Knockdown of mitochondria fusion factors and mitochondrial morphology proteins, EndoB and Letm1, impaired ATP synthesis in mitochondria. In these spermatocytes, cell growth was inhibited. Similar growth inhibition was observed upon knockdown of blw, which encodes an ATP synthase. Therefore, ATP depletion caused by inhibiting fusion factors and morphology proteins may result in growth inhibition. ATP is synthesized more efficiently in elongated mitochondria formed via these factors (Mitra et al., 2009). It is reasonable to speculate that inhibition of this process led to a decrease in ATP levels and cell growth inhibition. In ATP-depleted cells, AMPK activity increases, and inhibiting Tsc2 in the insulin-like peptides (ILP)-induced pathway eventually reduces protein synthesis (Inoki et al., 2003). Activation of the signaling pathways by ILPs is required for cell growth before meiosis (Ueishi et al., 2009). Consistently, when mitochondrial dynamics are disturbed in yeast and mammalian cells, ATP synthesis ceases (Wong et al., 2000; Parone et al., 2008). Therefore, inhibition of elongated mitochondrial structures, formed via mitochondrial fusion factors and morphology proteins, may have led to a decrease in ATP levels, resulting in cell growth impairments in spermatocytes. In normal cells, elongated mitochondria were observed in the polar spermatocyte

 doi:10.20944/preprints202509.0318.v1

stage (S2b). During the subsequent apolar stage (S3–S5), the spermatocyte growth becomes most active. Before the stages, ATP required for these processes may be efficiently synthesized within the elongated network structure. Alternatively, it may not be simply due to a reduction in ATP levels. In mammalian cells harboring the fragmented mitochondria, oxidative phosphorylation decreases while ROS production increases (Lunova et al., 2024). ROS may also influence the progression of the growth phase. Further investigation is needed to clarify this speculation.

3.4. Elongated Mitochondria Networks Are Transferred to Daughter Cells While Maintaining the Structures, Depending on Microtubules and F-Actin in Male Meiosis

In the interphase of mammalian cultured cells, mitochondria form an interconnected tubular network, and their membrane potential increases from G1 to S phase and at the G2/M phase (Mitra et al., 2009). Subsequently, mitochondria undergo fission before the M phase. This is assumed to facilitate the equal partition of mitochondria (Labbé et al., 2014). In contrast, we demonstrated that the mitochondrial network structure is established in spermatocytes and is transferred while maintaining its structure in meiosis. Compared to the shortened forms (where ATP synthesis is suppressed), the fused forms allow ATP to be supplied when it is needed. This is beneficial during the ATP-dependent dynamic stages of cell growth phase and subsequent M-phase. Additionally, the interconnected structure may facilitate equal distribution of the organelles during meiosis. After that, the organelles quickly cluster together to create Nebenkern. In mitosis, even if one of the two daughter cells receives an insufficient number of mitochondria, they can be amplified during the next S phase. In contrast, meiosis lacks a subsequent cell cycle to compensate for the insufficiency. To prevent this, a control mechanism might exist that guarantees equal mitochondrial partitioning.

Microtubules and F-actin play indispensable roles in transporting mitochondria to specific sites in mitotic cells and neurons (Chung et al., 2016; Lawrence et al., 2016). Consistently, mitochondria are transferred into two daughter cells in male meiosis, while being closely associated with aster and central spindle microtubules (Ichihara et al., 2007, live analysis in this study). F-actin also plays an indispensable role in accumulating these organelles next to the nucleus at the S2b, and in moving along microtubules and clustering at the cell equator during meiosis. The roles of these cytoskeletons in transporting mitochondria are consistent with findings in mammalian cells (Madan et al., 2022). Unexpectedly, even after microtubules were depolymerized, the mitochondrial network was maintained, and no significant changes in its distribution were observed in meiosis. This may be inconsistent with reports on mitosis in mammalian cells (Jones and Naylor, 2022). In Drosophila male meiosis, once the mitochondrial network is formed, the structure may be maintained without disintegrating even in the absence of microtubules. Each mitochondrion in the network may be interconnected with others during meiosis. Alternatively, another intracellular structure may bundle mitochondria. F-actin may play a significant role in the clustering and movement of the organelles.

3.5. The Establishment of the Mitochondrial Network Structure, Formed via Fusion Factors and Morphology Proteins, Plays Important Roles in the Execution of Male Meiosis

This study demonstrated that the network structure composed of elongated mitochondria is established before Drosophila male meiosis and is transferred to daughter cells, maintaining their network structures. This distribution differs from that in mitosis. When we depleted the fusion factors and the morphology proteins, EndoB and Letm1, we observed abnormal spermatid cysts consisting of only 16 cells. This phenotype has been observed in other mutants, in which the first and second meiosis do not occur (White-Cooper et al.,1993; Tanabe et al., 2017; Okazaki et al., 2020). The inhibition of fusion factors results in a shift in the fission/fusion balance toward fission, and the resultant inability to form a network structure leads to fewer meiotic cells. On the other hand, in testes where the fission factor Drp1 was down-regulated, but not in testes with Drp1 knockdown, abnormal spermatid cysts derived from a single meiosis were also observed, albeit at a lower frequency. Therefore, the fission factor may also play a role in male meiosis through maintaining the fusion/fission balance.

 doi:10.20944/preprints202509.0318.v1

Moreover, these abnormal cells in spermatid cysts, consisting of 16 or 32 cells, possessed two or more nuclei smaller than nuclei containing diploid chromosome complements. In the absence of meiosis I initiation, chromosome segregation does not happen (White-Cooper et al., 1993), and multiple nuclei should not form. This phenotype bears a striking resemblance to a mutant phenotype in which chromosome separation commences, yet is abruptly halted during anaphase, consequently resulting in the formation of nuclei at the sites of the chromosomes (Tanabe et al., 2019). When the elongated structure is disrupted, meiosis initiates but may fail to complete at the appropriate time. In primary spermatocytes with knockdown of factors involved in mitochondrial dynamics, the CycB accumulation at the onset was less pronounced than in controls. No nuclear transport of CycB, and consistently, no prominent anti-MPM2 immunostaining was observed. In the knockdown cells, the onset of meiosis may have been delayed compared to controls. To verify the possibility, it is necessary to observe meiotic cells; however, we were unable to find typical meiotic cysts. In mouse oocytes, the Drp1-knockdown also affects the restart of meiosis (Udagawa et al., 2014). Considering this consistent finding, we speculate that the inhibition of mitochondrial network formation led to the absence of CycB expression. The timing of CycB expression is determined by transcriptional control and the release of mRNA translation inhibition (Baker et al., 2023). In future studies, it will be important to investigate whether Rbp4 and Fest proteins (Baker et al., 2015), which regulate CycB translation, are affected by the knockdown of the fusion factors. In the ATP synthetase-knockdown spermatocytes, meiosis is completed (Sawyer et al., 2017, this study). Therefore, impaired ATP synthesis in mitochondria is not a direct cause of failure and abnormalities in meiosis. This study does not clearly explain why the knockdown of the factors involved in mitochondrial morphological changes impacts chromosome segregation during meiosis. This is a limitation of the current research. Since mitochondria are essential organelles in spermatogenesis, not only in Drosophila but also in mammals, our findings can provide important insights into the roles of mitochondrial dynamics in cell division and differentiation of male germ line cells.

4. Materials and Methods

4.1. Drosophila Stocks

w^{1118} (*w*) was used as a normal control stock. For the silencing of mRNAs for dynamic factors for mitochondria and the related proteins, the following *UAS-RNAi* stocks were used; *P{GD11094}v40478* (#40478) (hereinafter referred to as *UAS-MarfRNAi*^{GD})(from Vienna *Drosophila* Resource Center (VDRC), Vienna, Austria) (Poole et al., 2008), *P{JF01650}*(*UAS-MarfRNAi*^{JF}) (from Bloomington Drosophila Stock Center (BDSC)(Indiana University, Bloomington, IN, USA))(Ratnaparkhi, 2013), *P{KK106290}VIE-260B*(v107599)(*UAS-Opa1RNAi*^{KK})(v106290)(from VDRC)(Shin et al., 2024), *P{HMS00349}*(*UAS-Opa1RNAi*) (from BDSC)(Yang et al., 2013), *UAS-Drp1 RNAi* ^{JF02762} (*UAS-Drp1RNAi*^{JF})(Sênos Demarco, et al., 2019), *P{GD2208}*(*UAS-Letm1RNAi*^{GD}) (v6662)(from VDRC) (Schnorrer, et al., 2010), *P{TRiP.HMS01644}* (*UAS-Letm1RNAi*^{HMS})(from BDSC)(Li et al., 2020), *P{GD14693}*(*UAS-EndoBRNAi*^{GD})(v29293)(from VDRC)(Zhu, et al., 2013), *P{KK107885}VIE-260B}*(*UAS-EndoBRNAi*^{KK}) (v104712 from VDRC). To induce ectopic expression of dsRNAs against the relevant mRNAs, we used *P{UAS-Dcr2}*; *P{bam-GAL4::VP16}* (hereinafter abbreviated as *bam-GAL4*) for spermatocyte-specific *RNAi* experiments (Kitazawa et al., 2012). Thus, spermatocytes carrying *UAS-XRNAi*$^{\#}$, *P{UAS-Dcr2}* and *P{bam-GAL4::VP16}*, in which the relevant mRNA for the gene X is depleted, are denoted as *XRNAi*$^{\#}$. As a control, F1 males between *bam-Gal4* and wild-type (*bam*>+) were used. To visualize microtubules, *P{Ubi-tub56D-GFP}* (*GFP-tubulin*) was used (Inoue et al., 2004). We used *M{UAS-CycB.ORF.3xHA}* (#F001154, Fly-ORF; University of Zurich, Zurich, Switzerland) for the overexpression of Cyclin B (Yamazoe et al., 2023). For a downregulation of Drp1, its dominant negative mutant protein was also induced using *P{UAS-Drp1*^{K38A}*}*(*UAS-Drp1*^{DN})(a gift from J. Chung (Seoul National Univ.)(Park, et al., 2009). *P{bam-GAL4::VP16}* was used as a Gal4 driver for spermatocyte-specific induction of gene expression (Hayashi et al., 2016). *sa* (Lin et al., 1996, #1762, BDSC) and *twe* (White-Cooper et al., 1993, #4274, BDSC) mutants, whose male meiosis does not take

 doi:10.20944/preprints202509.0318.v1

place, were used as controls. All *Drosophila* stocks were maintained on standard cornmeal food at 25 °C as previously described (Oka et al., 2019). To maintain the stocks and obtain adults for aging-related experiments, the following standard cornmeal fly food was prepared: Per liter of water, 40 g of dried yeast (Asahi Group, Tokyo, Japan), 40 g of corn flour (Nippun, Tokyo, Japan), 100 g of glucose (Kato Chemical, Aichi, Japan), and 7.2 g of agar powder (Matsuki Agar, Nagano, Japan) were added, and 5 mL of a 10% methyl para hydroxybenzoate solution and 5 mL of propionic acid (Tokyo Kasei Kogyo, Tokyo, Japan) were added to 1L of the fly food. For an efficient induction of GAL4-dependent gene expression, individuals carrying the GAL4 driver gene and UAS transgenes were raised at 28 °C. Other experiments and stock maintenance were conducted at 25 °C.

4.2. Preparation of Post-Meiotic Spermatid Cysts

To estimate whether two consecutive meiotic divisions were executed correctly, we observed nuclei in post-meiotic spermatids at the onion stage just after the completion of meiosis II under phase-contrast microscopy, as previously described (Inoue et al., 2004; Tanabe et al., 2017). A pair of testes from pharate adults or newly eclosed adult flies (within 1 day old) was dissected to isolate spermatocyte cysts in Testis buffer (183 mM KCl, 47 mM NaCl, 10 mM EDTA, pH 6.8) and covered with a coverslip (Matsunami Co., Osaka, Japan) to flatten the cysts. To observe spermatids under a phase-contrast microscope, the cysts collected from the testes were mildly flattened in Testis buffer under a cover slip. After removing the coverslips, we transferred them into 100% methanol for 3 min at −30 °C to fix the samples. Subsequently, they were rehydrated in PBS (137.0 mM NaCl, 2.7 mM KCl, 10.1 mM $Na_2HPO_4 \cdot 12H_2O$, 1.8 mM KH_2PO_4), and then the DNA was stained with DAPI. Samples were observed using a phase-contrast microscope (Olympus, Tokyo, Japan, model: IX81). Normal spermatocytes undergo two meiotic divisions to form 64 spermatocytes simultaneously. The resultant spermatid possesses a one-to-one ratio of nucleus to mitochondrial aggregates, known as Nebenkerns (Fuller, 1993; Tanabe et al., 2017).

4.3. Drug Administration to the Testis Cells

To inhibit microtubule polymerization, testes from young adult flies were dissected in 50 μM/ml colchicine (# W01W0103-0385 (WAKO Pure Chemicals, Osaka, Japan)) in testis buffer and incubated for 15 min before fixation. For inhibition of actin-filament polymerization, testes from adult flies were dissected in 100 μM latrunculin A in testis buffer for 45 min before fixation. Testes squashes to evaluate onion-stage spermatids were performed as described above and viewed under phase-contrast microscopy.

4.4. Immunostaining of Testis Cells

Testis cells, collected from the testes as described above, were fixed in ethanol at −30 °C for 10 min, followed by fixation in 3.7% formaldehyde for 7 min. The slides were permeabilized in PBST (PBS containing 0.01% Triton-X) for 10 min and blocked with 10% normal goat serum in PBS. The following primary antibodies were used at the dilutions described: MPM-2 antibody (05-368, Sigma-Aldrich, St. Louis, MO, USA), 1/200; anti-Complex V alpha-subunit monoclonal antibody (#439800, Thermo Fisher, Waltham, MA, USA), 1/400; anti-Cyclin B monoclonal antibody (Developmental Studies Hybridoma Bank, Iowa City, IA, 1/200. After incubating with the primary antibody overnight at 4 °C, the fixed samples were repeatedly washed in PBS and subsequently incubated with anti-mouse or anti-rabbit IgG conjugated with Alexa Fluor 488 or 555 (Thermo Fisher, Waltham, MA, USA). After washing in PBS, they were mounted with VECTASHIELD Mounting Medium with DAPI (Vector Laboratories, Burlingame, CA, USA) and observed under IX81 fluorescent microscope (Olympus, Tokyo, Japan). Image acquisition was controlled using MetaMorph software version 7.6 (Molecular Devices, SAN Jose, CA, USA).

4.5. ATP Assay

 doi:10.20944/preprints202509.0318.v1

Ten pairs of testis were homogenized in the cell lysis buffer (10 mM Tris (pH 7.5), 100mM NaCl, 1 mM EDTA, 0.01% Triton X-100) on ice. These homogenates were immediately frozen in liquid nitrogen and subsequently inactivated at 99 °C for 3 min. After centrifugation at 6010× *g* for 10 min, the ATP levels were quantified in the supernatants using the ATP Determination Kit (#A22066, Invitrogen, Waltham, MA, USA). The fluorescence intensity was measured using a luminometer (Lumat LB9507, Berthold Technologies, Bad Wildbad, Germany). Based on the standard curve created, the ATP levels of the samples were determined. Protein concentration was measured using the Qubit 2.0 Fluorometer (Invitrogen, Waltham, MA, USA) and calculated as ATP [mM]/Protein [mg].

4.6. Transmission Electron Microscope Observation of Adult Testes

Abdomens of young male flies (within two days after eclosion) were placed in fixative solution (4% paraformaldehyde, 2% glutaraldehyde in 0.1 M cacodylate buffer, pH = 7.4), as previously reported (Ozaki et al., 2022). The fixed specimens were washed with 0.1 M cacodylate buffer and treated with 2% osmium tetroxide in 0.1 M cacodylate buffer. The specimens were dehydrated by consecutive incubation in 50%, 70%, 90%, and 100% ethanol. After the specimens were infiltrated with propylene oxide and put into a 7:3 mixture of propylene oxide and resin (Quetol-812, Nisshin EM Co., Tokyo, Japan), they were transferred to new resin and polymerized. The specimens in the polymerized resins were ultrathin sectioned at 70 nm using Ultracut-UCT (Leica, Vienna, Austria) and mounted on copper grids. After staining with 2% uranyl acetate, the sections were washed with distilled water and stained with lead stain solution (Sigma-Aldrich Co., Tokyo, Japan). The grids were observed using a transmission electron microscope (JEM-1400Plus, JEOL Ltd., Tokyo, Japan) at 100 kV acceleration voltage and photographed with a CCD camera (EM-14830RUBY2, JEOL Ltd., Tokyo, Japan).

4.7. Statistical Analysis

Each dataset comparing the control and each knockdown was statistically assessed using Student's *t*-test, as described in a previous study (Azuma et al., 2021). Data were considered significant at *p*-values < 0.05. Statistical analyses were performed using Excel (version 16.78.3, Redmond, WA, USA) and GraphPad Prism 9 (GraphPad Software, San Diego, CA, USA).

Supplementary Materials: The following supporting information can be downloaded at the website of this paper posted on Preprints.org, Figure S1:; Figure S2: Figure S3:; Figure S4:.

Author Contributions: Formal analysis and investigation: T. M.,Y.H.I., M.Y.; writing—original draft: T.M. and Y.H.I.; writing—review and editing: Y.H.I.; project administration: Y.H.I.; funding acquisition: Y.H.I.; visualization: Y.H.I.; supervision: Y.H.I. All authors have read and agreed to the published version of the manuscript.

Funding: This study was partially funded by a JSPS KAKENHI Grant-in-Aid for Scientific Research C, grant number of JSPS (JP26440188), awarded to Y.H.I.

Institutional Review Board Statement: The animal study protocol was approved by the Kyoto Institute of Technology Review Board (protocol code: R4-11 and date of approval: January 24 2023).

Informed Consent Statement: Not applicable.

Data Availability Statement: The datasets generated and/or analyzed in the current study are available from the corresponding author upon reasonable request.

Acknowledgments: We thank R. Awane and H. Etoh (Kyoto Institute of Technology) for their technical assistance, J. Chung (Seoul National Univ.), Bloomington Drosophila Stock Center and Vienna Drosophila RNAi Center for providing fly stock, and DSHB (Iowa univ.) for providing the anti-CycB antibody. We acknowledge Tokai Electron Microscopy Co. (Nagoya, Japan) for their help with TEM observation.

 doi:10.20944/preprints202509.0318.v1

Conflicts of Interest: The authors declare no conflicts of interest.

References

Aldridge, A.C.; Benson, L.P.; Siegenthaler, M.M.; Whigham, B.T.; Stowers, R.S.; Hales, K.G. Roles for Drp1, a dynamin-related protein, and milton, a kinesin-associated protein, in mitochondrial segregation, unfurling and elongation during Drosophila spermatogenesis. *Fly* (*Austin*), 2007, *1*, 38–46.

Azuma, M.; Ogata, T.; Yamazoe, K.; Tanaka, Y.; Inoue, Y.H. Heat shock cognate 70 genes contribute to Drosophila spermatocyte growth progression possibly through the insulin signaling pathway. *Dev. Growth Differ*. 2021, *63*, 231-248.

Baker, C.C.; Gim, B.S.; Fuller, M.T. Cell type-specific translational repression of Cyclin B during meiosis in males. *Development*. 2015,*142*, 3394-402.

Benard, G.; Bellance, N.; James, D.; Parrone, P.; Fernandez, H.; Letellier, T.; Rossignol, R. Mitochondrial bioenergetics and structural network organization. *J. Cell. Sci.* 2007, *120*, 838–848.

Bereiter-Hahn, J.; Vöth, M. Dynamics of mitochondria in living cells: shape changes, dislocations, fusion, and fission of mitochondria. *Microsc. Res. Tech*. 1994, *27*, 198–219.

Cenci, G.; Bonaccorsi, S.; Pisano, C.; Verni, F.; Gatti, M. Chromatin and microtubule organization during premeiotic, meiotic and early postmeiotic stages of Drosophila melanogaster spermatogenesis. *J. Cell. Sci.* 1994, *107*, 3521–3534.

Chen, H.; Detmer, S.A.; Ewald, A.J.; Griffin, E.E.; Fraser, S.E.; Chan, D.C. Mitofusins Mfn1 and Mfn2 coordinately regulate mitochondrial fusion and are essential for embryonic development. *J Cell Biol*, 2003.*160*, 189–200.

Chen, H.; Vermulst, M.; Wang, Y.E.; Chomyn, A.; Prolla, T.A.; McCaffery, J.M.; Chan, D.C. Mitochondrial fusion is required for mtDNA stability in skeletal muscle and tolerance of mtDNA mutations. *Cell* 2010, *141*, 280–289.

Cho, M.J.; Kim, Y.J.; Yu, W.D.; Kim, Y.S.; Lee, J.H. Microtubule Integrity Is Associated with the Functional Activity of Mitochondria in HEK293. Cells. 2021, *10*, 3600.

Chung, J.Y.; Steen, J.A.; Schwarz, T.L. Phosphorylation-Induced Motor Shedding Is Required at Mitosis for Proper Distribution and Passive Inheritance of Mitochondria. *Cell Rep*. 2016, *16*, 2142-2155.

Davies, V.J.; Hollins, A.J.; Piechota, M.J.; Yip, W.; Davies, J.R.; White, K.E.; Nicols, P.P.; Boulton, M.E.; Votruba, M. Opa1 deficiency in a mouse model of autosomal dominant optic atrophy impairs mitochondrial morphology, optic nerve structure and visual function. *Hum. Mol. Genet.* 2007, *16*, 1307–1318.

Deng, H.; Dodson, M.W.; Huang, H.; Guo, M. The Parkinson's disease genes pink1 and parkin promote mitochondrial fission and/or inhibit fusion in Drosophila. *Proc. Natl. Acad. Sci. U.S.A.* 2008, *105*, 14503–14508.

Eura, Y.; Ishihara, N.; Yokota, S.; Mihara, K. Two Mitofusin proteins, mammalian homologues of FZO, with distinct functions are both required for mitochondrial fusion. *J. Biochem.* 2003, *134*, 333–344.

Fuller, M.T. (1993). Spermatogenesis. In The development of *Drosophila melanogaster*. Bate M., Martinez Arias, A., Eds.; Cold Spring Harbor Laboratory Press, NewYork, USA, 1993, pp. 71–147.

Hales, K.G.; Fuller, M.T. Developmentally regulated mitochondrial fusion mediated by a conserved, novel, predicted GTPase. *Cell* 1997, *90*, 121–129.

Hayashi, D.; Tanabe, K.; Katsube, H.; Inoue, Y.H. B-type nuclear lamin and the nuclear pore complex Nup107-160 influences maintenance of the spindle envelope required for cytokinesis in Drosophila male meiosis. *Biol. Open* 2016, *5*, 1011-1021.

Hinton, A. Jr.; Katti, P.; Christensen, T.A.; Mungai, M., Shao, J.; Zhang, L.; Trushin, S.; Alghanem A, Jaspersen A, Geroux RE, Neikirk K, Biete M, Lopez EG, Shao B, Vue Z, Vang L, Beasley HK, Marshall AG, Stephens D, Damo S, Ponce J, Bleck CKE, Hicsasmaz I, Murray SA, Edmonds RAC, Dajles A, Koo YD, Bacevac S, Salisbury JL, Pereira, R.O.; Glancy, B.; Trushina, E.; Abel, E.D. A Comprehensive Approach to Sample Preparation for Electron Microscopy and the Assessment of Mitochondrial Morphology in Tissue and Cultured Cells. *Adv. Biol. (Weinh)* 2023, *7*, e2200202.

Hirusaki, K.; Yokoyama, K.; Cho, K.; Ohta, Y. Temporal depolarization of mitochondria during M phase. *Sci. Rep.* 2017, *7*, 16044.

 doi:10.20944/preprints202509.0318.v1

Ichihara, K.; Shimizu, H.; Taguchi, O.; Yamaguchi, M.; Inoue, Y.H. A *Drosophila* orthologue of Larp protein family is required for multiple processes in male meiosis. *Cell Struct. Funct.* 2007, *32*, 89–100.

Inoue, Y.H.; Savoian, M.S.; Suzuki, T.: Máthé, E.; Yamamoto, M.T.; Glover, D.M. Mutations in orbit/mast reveal that the central spindle is comprised of two microtubule populations, those that initiate cleavage and those that propagate furrow ingression. *J. Cell Biol.* 2004, 166, 49-60.

Inoue, Y. H.; Miyauchi, C.; Ogata, T.; Kitazawa, D. Dynamic alteration of cellular component of male meiosis in Drosophila. In Meiosis, A. Swan, Eds.; Intech Open, 2012; pp. 67-86.

Inoki, K.; Zhu, T.; Guan, K.-L. TSC2 Mediates cellular energy response to control cell growth and survival. *Cell* 2003, *115*, 577–590.

Ishihara, N.; Jofuku, A.; Eura, Y.; Mihara, K. Regulation of mitochondrial morphology by membrane potential, and DRP1-dependent division and FZO1-dependent fusion reaction in mammalian cells. *Biochem. Biophys. Res. Commun.* 2003, *301*, 891–898.

Ishihara, N.; Nomura, M.; Jofuku, A.; Kato, H.; Suzuki, S.O.; Masuda, K.; Otera, H.; Nakanishi, Y.; Nonaka, I.; Goto, Y. Mitochondrial fission factor Drp1 is essential for embryonic development and synapse formation in mice. *Nat. Cell Biol*. 2009, *11*, 958–966.

Jourdain, I.; Gachet, Y.; Hyams, J.S. The dynamin related protein Dnm1 fragments mitochondria in a microtubule-dependent manner during the fission yeast cell cycle. *Cell Motil. Cytoskeleton*. 2009, *66*, 509-23.

Jones, M.D.; Naylor, K. Simple to Complex: The Role of Actin and Microtubules in Mitochondrial Dynamics in Amoeba, Yeast, and Mammalian Cells. *Int. J. Mol. Sci*. 2022, *23*, 9402.

Karbowski, M.; Jeong, S.-Y.; Youle, R.J. Endophilin B1 is required for the maintenance of mitochondrial morphology. *J. Cell Biol.* 2004, *166*, 1027–1039.

Kitazawa, D.; Yamaguchi, M.; Mori, H.; Inoue, Y.H. COPI-mediated membrane trafficking is required for cytokinesis in Drosophila male meiotic divisions. *J Cell Sci.* 2012, *125*, 3649-60.

Labbé, K.; Murley, A.; Nunnari, J. Determinants and functions of mitochondrial behavior. *Annu. Rev. Cell Dev. Biol.* 2014, *30*, 357-391.

Lawrence, E.J.; Boucher, E.; Mandato, C.A. Mitochondria-cytoskeleton associations in mammalian cytokinesis. *Cell Div*. 2016, *11*:3.

Li, S.; Wu, Z.; Li, Y.; Tantray, I.; De Stefani, D.; Mattarei, A.; Krishnan, G.; Gao, F.B.; Vogel, H.; Lu, B. Altered MICOS Morphology and Mitochondrial Ion Homeostasis Contribute to Poly(GR) Toxicity Associated with C9-ALS/FTD. *Cell Rep*. 2020, *32*, 107989.

Liesa, M.; Palacín, M.; Zorzano, A. Mitochondrial dynamics in mammalian health and disease. *Physiol. Rev*. 2009, *89*, 799–845.

Lin, T.Y.; Viswanathan, S.; Wood, C.; Wilson, P.G.; Wolf, N.; Fuller, M.T. Coordinate developmental control of the meiotic cell cycle and spermatid differentiation in Drosophila males. Development 1996, *122*, 1331-1341.

Lunova, M.; Jirsa, M.; Dejneka, A.; Sullivan, G.J.; Lunov, O. Mechanical regulation of mitochondrial morphodynamics in cancer cells by extracellular microenvironment. *Biomater. Biosyst.* 2024, *14*, 100093.

Madan, S.; Uttekar, B.; Chowdhary, S.; Rikhy, R. Mitochondria Lead the Way: Mitochondrial Dynamics and Function in Cellular Movements in Development and Disease. *Front. Cell Dev. Biol.* 2022, *9*, 781933.

Mattenberger, Y.; James, D.I.; Martinou, J.-C. Fusion of mitochondria in mammalian cells is dependent on the mitochondrial inner membrane potential and independent of microtubules or actin. *FEBS. Letters* 2003, *538*, 53–59.

McQuibban, G.A.; Lee, J.R.; Zheng, L.; Juusola, M.; Freeman, M. Normal mitochondrial dynamics requires rhomboid-7 and affects Drosophila lifespan and neuronal function. *Curr. Biol.* 2006, *16*, 982-989.

Mitra, K.; Rikhy, R.; Lilly, M.; Lippincott-Schwartz, J. DRP1-dependent mitochondrial fission initiates follicle cell differentiation during Drosophila oogenesis. *J. Cell Biol.* 2012, *197*, 487–497.

Nakamura, S.; Matsui, A.; Akabane, S. et al. The mitochondrial inner membrane protein LETM1 modulates cristae organization through its LETM domain. *Commun. Biol.* 2020, *3*, 99.

Oka, S.; Hirai, J.; Yasukawa, T.; Nakahara, Y.; Inoue, Y.H. A correlation of reactive oxygen species accumulation by depletion of superoxide dismutases with age-dependent impairment in the nervous system and muscles of Drosophila adults. *Biogerontol*. 2015, *16*, 485-501.

 doi:10.20944/preprints202509.0318.v1

Okamoto, K.; Shaw, J.M. Mitochondrial morphology and dynamics in yeast and multicellular eukaryotes. *Annu. Rev. Genet.* 2005, *39*, 503–536.

Okazaki, R.; Yamazoe, K.; Inoue, Y.H. Nuclear Export of Cyclin B Mediated by the Nup62 Complex Is Required for Meiotic Initiation in Drosophila Males. *Cells* 2020, *9*, 270.

Ozaki, M.; Le, T.D.; Inoue, Y.H. Downregulating mitochondrial DNA polymerase γ in the muscle stimulated autophagy, apoptosis, and muscle aging-related phenotypes in Drosophila adults. Biomolecules 2022, *12*, 1105.

Park, J.; Lee, G.; Chung, J. The PINK1-Parkin pathway is involved in the regulation of mitochondrial remodeling process. *Biochem. Biophys. Res. Commun.* 2009, *37*, 518-523.

Parone, P.A.; Da Cruz, S.; Tondera, D.; Mattenberger, Y.; James, D.I.; Maechler, P.; Barja, F.; Martinou, J.-C. Preventing mitochondrial fission impairs mitochondrial function and leads to loss of mitochondrial DNA. *PLoS ONE* 2008, *3*, e3257.

Poole, A.C.; Thomas, R.E.;Yu, S.; Vincow, E.S.; Pallanck, L. The mitochondrial fusion-promoting factor mitofusin is a substrate of the PINK1/parkin pathway. *PLoS ONE* 2010, *5*, e10054.

Ratnaparkhi, A. Signaling by Folded gastrulation is modulated by mitochondrial fusion and fission. *J. Cell Sci.* 2013, *126*, 5369-5376.

Sauvanet, C.; Duvezin-Caubet, S.; di Rago, J.-P.; Rojo, M. Energetic requirements and bioenergetic modulation of mitochondrial morphology and dynamics. *Semin. Cell Dev. Biol.* 2010, *21*, 558–565.

Sawyer, E.M.; Brunner, E.C., Hwang, Y.; Ivey, L,E,; Brown, O.; Bannon, M.; Akrobetu, D.; Sheaffer, K.E.; Morgan, O.; Field, C.O.; Suresh, N.; Gordon, M.G.; Gunnell, E.T.; Regruto, L.A.; Wood, C.G.; Fuller, M.T.; Hales, K.G. Testis-specific ATP synthase peripheral stalk subunits required for tissue-specific mitochondrial morphogenesis in Drosophila. *BMC Cell Biol.* 2017, *18*, 6.

Schnorrer, F.; Schönbauer, C.; Langer, C.C.; Dietzl, G.;Novatchkova, M.; Schernhuber, K.; Fellner, M.; Azaryan, A.; Radolf, M.; Stark, A.; Keleman, K.; Dickson, B.J. Systematic genetic analysis of muscle morphogenesis and function in Drosophila. *Nature* 2010, *464*, 287-291.

Sênos Demarco, R.; Uyemura, B.S.; D'Alterio, C.; Jones, D.L. Mitochondrial fusion regulates lipid homeostasis and stem cell maintenance in the Drosophila testis. *Nat. Cell Biol.* 2019, *21*, 710-720.

Stephan, T.; Ilgen, P.; Jakobs, S. Visualizing mitochondrial dynamics at the nanoscale. *Light Sci. Appl.* 2024, *13*, 244.

Taguchi, N.; Ishihara, N.; Jofuku, A.; Oka, T.; Mihara, K. Mitotic phosphorylation of dynamin-related GTPase Drp1 participates in mitochondrial fission. *J. Biol. Chem.* 2007, *282*, 11521-11529.

Tanabe, K.; Okazaki, R.; Kaizuka, K.; Inoue, Y.H. Time-lapse Observation of Chromosomes, Cytoskeletons and Cell Organelles during Male Meiotic Divisions in Drosophila. *Bio Protoc.* 2017, *7*, e2225.

Tanabe, K.; Awane, R.; Shoda, T.; Yamazoe, K.; Inoue, Y.H. Mutations in mxc tumor-suppressor gene induce chromosome instability in Drosophila male meiosis. *Cell Struct. Funct.* 2019, *44*, 121-135.

Trevisan, T.; Pendin, D.; Montagna, A.; Bova, S.; Ghelli, A.M.; Daga, A. Manipulation of Mitochondria Dynamics Reveals Separate Roles for Form and Function in Mitochondria Distribution. *Cell Rep.* 2018, *23*, 1742-1753.

Ueishi, S.; Shimizu, H.; Inoue, Y.H. Male germline stem cell division and spermatocyte growth require insulin signaling in *Drosophila*. *Cell Struct. Funct.* 2009, *34*, 61–69.

Udagawa, O.; Ishihara, T.; Maeda, M.; Matsunaga, Y.; Tsukamoto, S.; Kawano, N.; Miyado, K.; Shitara, H.; Yokota, S.; Nomura, M.; *et al*. Mitochondrial fission factor Drp1 maintains oocyte quality via dynamic rearrangement of multiple organelles. *Curr. Biol.* 2014, *24*, 2451–2458.

Vedelek, V.; Jankovics, F.; Zádori, J.; Sinka, R. Mitochondrial Differentiation during Spermatogenesis: Lessons from *Drosophila melanogaster*. *Int. J. Mol. Sci.* 2024, *25*, 3980.

Wakabayashi, J.; Zhang, Z.; Wakabayashi, N.; Tamura, Y.; Fukaya, M.; Kensler, T.W.; Iijima, M.; Sesaki, H. The dynamin-related GTPase Drp1 is required for embryonic and brain development in mice. *J. Cell Biol.* 2009, *186*, 805-816.

Westermann, B. Molecular machinery of mitochondrial fusion and fission. *J. Biol. Chem.* 2008, *283*, 13501-13505.

White-Cooper, H.; Alphey, L.; Glover, D.M. The cdc25 homologue twine is required for only some aspects of the entry into meiosis in Drosophila. *J Cell Sci.* 1993, *106*, 1035–1044.

 doi:10.20944/preprints202509.0318.v1

Wong, E.D.; Wagner, J.A.; Gorsich, S.W.; McCaffery, J.M.; Shaw, J.M.; Nunnari, J. The Dynamin-related GTPase, Mgm1p, is an intermembrane space protein required for maintenance of fusion competent mitochondria. *J. Cell Biol.* 2000, *151*, 341–352.

Yamazoe, K.; Inoue, Y.H. Cyclin B Export to the Cytoplasm via the Nup62 Subcomplex and Subsequent Rapid Nuclear Import Are Required for the Initiation of Drosophila Male Meiosis. Cells. 2023, *12*, 2611.

Yang, Y.; Hou, L.; Li, Y.; Ni, J.; Liu, L. Neuronal necrosis and spreading death in a Drosophila genetic model. *Cell Death Dis.* 2013, 4, e723.

Zhao, J., Lendahl, U., and Nistér, M. Regulation of mitochondrial dynamics: convergences and divergences between yeast and vertebrates. *Cell. Mol. Life Sci.* 2013, *70*, 951–976.

Zhu, J.Y.; Vereshchagina, N.; Sreekumar, V.; Burbulla, L.F.; Costa, A.C.; Daub, K.J.; Woitalla, D.; Martins, L.M.; Krüger, R.; Rasse, T.M. Knockdown of Hsc70-5/mortalin Induces Loss of Synaptic Mitochondria in a Drosophila Parkinson's Disease Model. PLoS ONE 2013, *8*, e83714.